Feasibility of Additive Manufacturing Method for Developing Stretchable and Flexible Embedded Circuits

A PLAN B PROJECT REPORT
SUBMITTED TO THE FACULTY OF THE GRADUATE SCHOOL
OF UNIVERSITY OF MINNESOTA
BY

Sachin Bijadi

IN PARTIAL FULFILLMENT OF THE REQUIREMENTS
FOR THE DEGREE OF
MASTER OF SCIENCE IN MECHANICAL ENGINEERING

Timothy Kowalewski, PhD

August, 2014

Acknowledgements

I would like to acknowledge the support and guidance of Dr. Timothy Kowalewski in achieving the fulfillment of this project. Sincere thanks to fellow researchers of the Medical Robotics and Devices Laboratory, John O'Neill, Timothy Zalusky, and Rodney Dockter II for not only assisting with various aspects of implementing this project but also for providing vital moral backing to help me in working towards my graduation.

Dedication

This work is dedicated to my friends and family who have supported me through various stages of my life and ensured that I always strived to achieve excellence in any task undertaken with the courage to travel off the beaten path.

Abstract

This work documents the development and testing of stretchable and flexible embedded circuits using additive manufacturing method. With the widespread popularity of desktop 3D printers, the power of low-cost 3D printing can be harnessed to print electronics on stretchable and flexible bio-compatible “skins” with integrated circuitry that can conform to irregularly-shaped mounting surfaces. A multi-material, freeform fabrication process with quick tool change provides the potential to print complete, electronically functional devices in a single manufacturing process, integrating the printing of both the structural and electronic blocks of the device. In this work, a custom-developed syringe-based closed-loop extrusion process using conductive silicone was developed for printing integrated circuits. The characteristics of the conductive silicone under stretching were studied. A proof-of-concept flexible bio-compatible ‘skin’ device with an embedded voltage divider circuit was printed and the behavior of the device was studied under various working conditions.

Table of Contents

List of Figures

Chapter 1

Introduction

1.1 Overview

Stretchable electronics constitute the creation of integrated circuits that can offer the electrical properties of conventional, rigid wafer-based technologies but with the ability to be stretched, compressed, twisted, bent, and deformed into arbitrary shapes. The ability to print low-resistance electrodes with fine resolution, and spanning three dimensions opens up many applications like flexible displays, RFID tags, antennas [1], sensor tapes, artificial skin and more. Stretchable electronics are also ideal for applications in biomedical systems like implants or smart clothes and wearable sensors, due to their capability to stretch and adapt to the movement of the mounting surface: either directly on the user or through a fabric-based substrate for mounting [2, 3, 4, 5].

The ability to print integrated circuits on flexible substrates enables attributes like conformity, lightweight structure and shock-resistant construction in electronic devices that are difficult to achieve with technologies that use semiconductor wafers or glass plates as substrates [6]. There has been tremendous progress in the past decade in the research and development of printable electronics on mechanically flexible substrates based on inorganic active components, which provide high performances and stable operation at low cost [3].

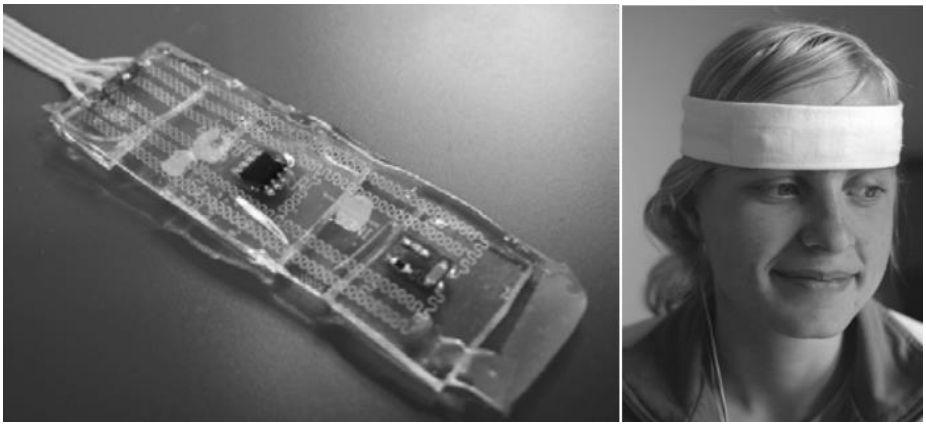

Figure 1: Stretchable thermometer for fever monitoring embedded in a wearable textile head band [7].

Some examples of stretchable sensors that have been developed in recent years include a new stretchable force sensor for hand force measurement developed by Abu-Khalaf et al., where optoelectronic components were embedded within a soft rubber substrate, connected by stretchable conductors which could conform to the two-dimensional curvature of the human finger [8]. This sensor was fabricated by depositing conductive metal lines on a pre-stretched rubber substrate.

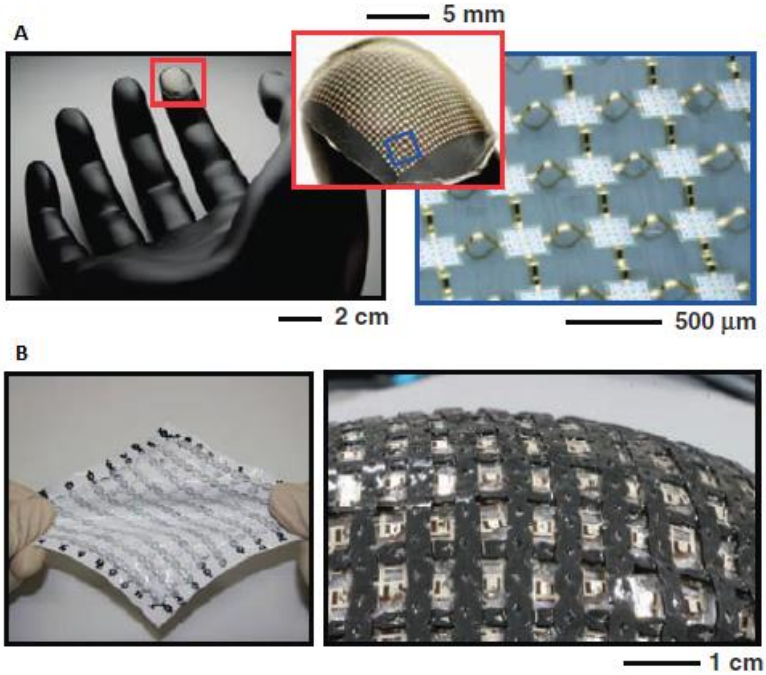

Figure 2: Examples of stretchable electronics: (A) Stretchable circuit with a mesh design, wrapped onto a model of a fingertip, shown at low (left), moderate (center) and high (right) magnification. (B) Array of organic transistors interconnected by elastic conductors on a sheet of polydimethylsiloxane (PDMS) in a stretched (left) and curvilinear (right) configuration [4].

Kramer et al. fabricated a hyperelastic, thin, transparent pressure sensitive keypad by embedding a rubber film with conductive liquid-filled microchannels (Figure 3). Applying pressure to the surface of the elastomer deforms the cross-section of underlying microchannels and changes the electrical resistance across the affected channels. [9]

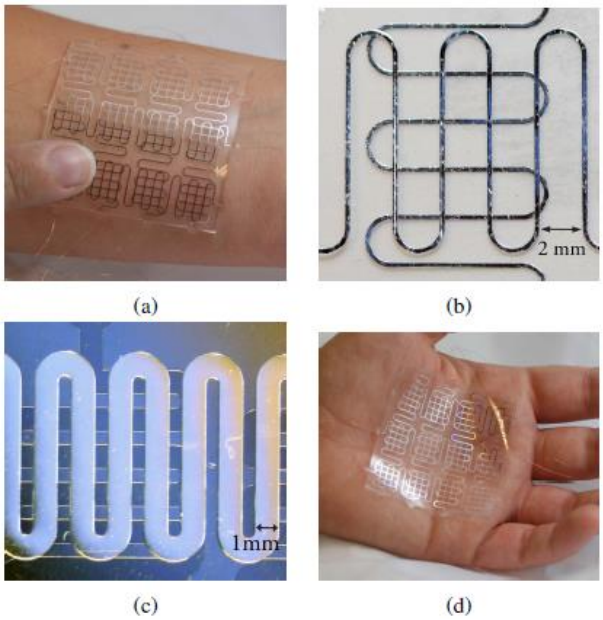

Figure 3: Thin sheets of PDMS matrix sheet embedded with conductive liquid-filled (eGaIn) microchannels for pressure sensing applications. (a) A twelve-key keypad resting on a wrist. (b) A single key of the keypad. (c) Conductive liquid-filled channels. (d) A twelve-key conformable keypad resting in the palm of a hand [9].

Traditional printing methods like screen-printing and inkjet printing produce low-aspect ratio features that need to be supported by an underlying substrate or device, constraining the patterning of in- or out-of-plane spanning elements [2]. This calls for a novel approach to printing stretchable electronics. In recent years additive manufacturing techniques have found wide-spread use both due to their reduced cost, increased accessibility as well as the ease of use. With the proliferation of low-cost effective desktop 3D printing more and more people have access to easy and efficient free-form fabrication of CAD designs with reduced complexity of infrastructure required. However most applications of additive manufacturing technologies are limited to manufacturing of non-conductive structures. Periard et al. explored integrating the 3D printing of both structural layers and electronic circuitry and developed a novel method to print fully-

functional, rigid electronic devices with a personal fabrication device (Fab@home Model 1 3D printer) using a multi-material fabrication approach [10].

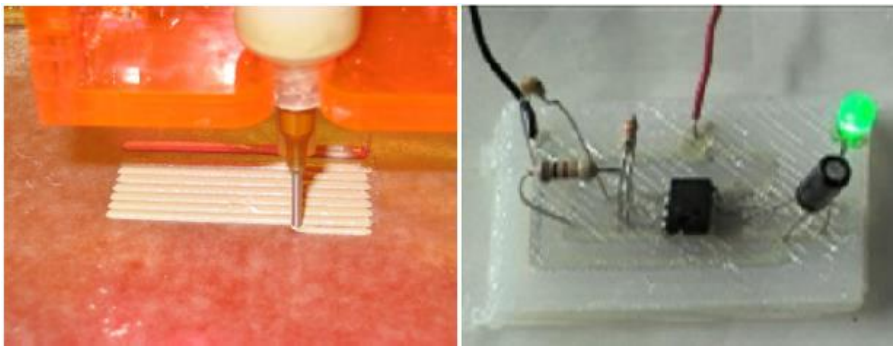

Figure 4: Printing conductive silicone traces with a 3D printer (left) and complete rigid integrated circuit [10].

Similarly, with advances in tissue engineering, additive manufacturing techniques have provided novel methods to effectively combine biological tissue and electronic components to 3D print bionic organs [11].

For this work moisture-accelerated RTV cure silicone with conductive silver nanoparticle fillings (provided by Silicone Solutions, OH) is used as the conductive ink printed over a substrate of clear non-conductive RTV silicone (provided by 7-Sigma Inc., MN). A proof-of-concept system using a syringe-based extrusion head with closed-loop PID extrusion velocity control is designed to extrude both conductive and non-conductive silicones. This head is designed to be mounted on to the arm of a custom 6-axis robot (CORVUS, Medical Robotics & Devices Laboratory, University of Minnesota [12]) which has the capability to detect and track irregular printing surfaces, allowing the 3D printing head to maneuver easily around the object to be printed on, thus providing the capability to print directly on to complex and irregular anatomical geometries unlike conventional 3-axis 3D printing systems.

1.2 Prior Work

Conductive printing materials

There are several options available for conductive materials that meet the requirements for printing stretchable electronics: conducting polymers, inorganic semiconductors and carbon nanotubes (shown below in Figure 5).

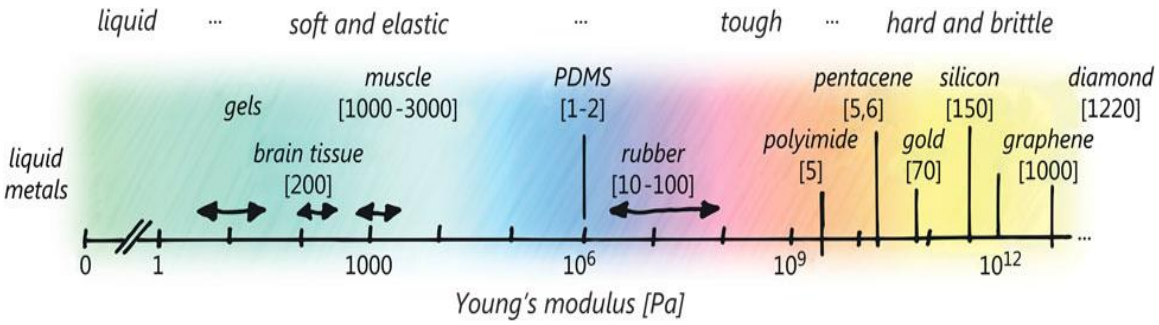

Figure 5: Stretchable electronic surfaces combine viscoelastic, plastic, and brittle materials with many orders of magnitude differences in Young's modulus. The materials range from liquid metals, gels, brain tissue, muscles, elastomers, polymers, metals, semiconductors, to carbon-based solids [13].

Many approaches use elastic conductors as electrical interconnects between active devices that are rigid or only bendable. Although carbon black-loaded elastomer-based conductive rubbers have been known for decades, their resistances and their dependence on strain are both too large to be useful. In a much more promising and recent approach, long, single-walled carbon nanotubes (SWNTs) serve as conductive dopants in a rubber matrix [4]. SWNTs processed by grinding in an ionic liquid and then mixing with a fluorinated copolymer yield a black, paste-like conductive substance. This material can be printed onto sheets of polydimethylsiloxane (PDMS) to yield elastic conducting traces with stretchability in the range of 100% (Figure 6).

A different, but related approach to physical vapor deposition (PVD) onto PDMS is the direct writing with a silver nanoparticle ink onto a flexible substrate yielding a wavy metallic microwire that can accommodate stretching through changes in wavelength and amplitude [4]. An ionic conductor is another possible candidate for a stretchable conductive material. Keplinger et al. demonstrated a transparent actuator that can generate large strains with the electromechanical transduction being achieved without an electrochemical reaction. Ionic conductors have higher resistivity than many electronic conductors; however, when large stretchability and high transmittance are required ionic conductors have lower sheet resistance than all existing electronic conductors [14].

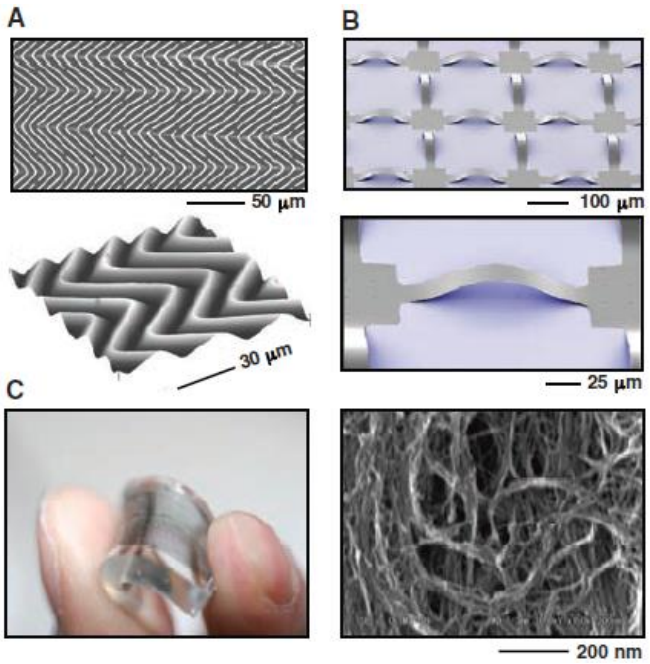

Figure 6: Concepts for stretchable electronic materials: (A) Stretchable silicon membrane (~100nm thickness) configured in a wavy shape and bonded to a piece of rubber, presented in optical (top) and atomic force (bottom) microscope images. (B) Extremely stretchable silicon membrane patterned into mesh geometry and bonded to rubber substrate at square pads located between arc-shaped bridge structures. (C) Stretchable conductive lines of a SWNT gel printed on a slab of rubber (left) where the networks of SWNTs provide electrical pathways in these composites [4].

Kim et al. demonstrated stretchable conductors of polyurethane containing spherical nanoparticles deposited by either layer-by-layer assembly or vacuum-assisted flocculation [15, 16]. The advantages of using nanoparticles for preparation of conductive material in stretchable electronics are:

a) Nanoparticles in a polymer matrix represent a more dynamic system that has greater freedom for reversible nanoscale restructuring: an essential property for stretchability.
b) Greater matrix mobility from nanoparticles than from nanotubes/nanowires. Any conducting pathways lost upon deformation could potentially be recovered in a different particle configuration.
c) Conductance between 2 nanoparticles does not depend on their mutual orientation.

While polyurethane based nanocomposites have been tested to be flexible and conductive making them a suitable candidate for stretchable electronics, they often require

sophisticated manufacturing processes and are more expensive [17]. Alternatively silicone with silver nanoparticles as conductive filler can be ideally used as a conductive material for 3D printing. Use of the nanoparticles induces conductivity in the otherwise inert silicone thereby providing a combination of good extrusion characteristics and mechanical properties while also being conductive [10]. Silicone is also a biocompatible material. This is a significant advantage rendering silicone a promising candidate for medical applications in this area.

Fabrication methods for stretchable electronics

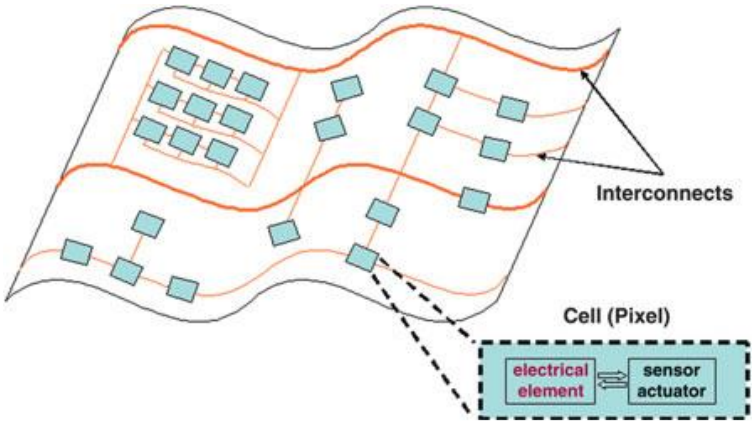

Figure 7: Architecture of an elastic electronic surface. Cells with optoelectronic functions are made on islands and are connected with flexible conductors on a flexible substrate [13].

Stretchable electronics are designed for uniaxial, biaxial, or radial stretching by tens of percent. However optoelectronic circuits contain brittle materials that will break if stretched by more than a few tenths of a percent. This leads to an architecture where the circuits are placed on platforms or islands which are mostly rigid in-plane and flexible out-of-plane as shown in Figure 7. The substrates exposed between the rigid islands along with the conducting traces that run across it, accommodate the elastic strain [13].

A common approach to fabrication of stretchable electronics is the creation of structures into “wavy” shapes and bonding them to elastomeric substrates yielding systems that can not only flex but also stretch and compress [18]. The Molded Interconnect Device (MID) technology uses rigid or flexible standard components that are interconnected by meander shaped metallic wires and embedded by molding in a stretchable substrate polymer [7, 19, 20, 21, 22]. This closely follows the standard PCB fabrication method.

In another approach, semiconductor nanowires (NWs) are used as versatile building blocks for flexible electronics, involving the chemical vapor deposition (CVD) growth of NWs followed by their transfer and assembly on flexible substrates [3]. Sekitani et al. used an ionic liquid of 1-butyl-3-methylimidazolium bis(trifluoromethanesulfonyl)imide, and uniformly dispersed SWNTs as chemically stable dopants in a vinylidene fluoride-hexafluoropropylene copolymer matrix to form a composite film which was coated with dimethylsiloxane-based rubber [23]. Park et al. developed a conductive composite mat of silver nanoparticles with rubber fibres that allowed the formation of highly stretchable circuits. A silver nanoparticle precursor is absorbed in electrospun poly (styrene-block-butadiene-block-styrene) (SBS) rubber fibres and then converted into silver nanoparticles directly in the fibre mat. Electric circuits are deposited directly on the electrospun fibre mat by nozzle printing, inkjet printing and spray printing of the precursor [24]. Aerosol Printing & Aerosol Jet Machining methods have also been employed to print electronics. Thompson et al. developed a custom aerosol printer to print a multiwall carbon nanotube solution onto an insulating flexible substrate to create a strain sensor [25].

Stretchable electronics are mostly fabricated with these planar technologies that have evolved from the materials and processes of classical microfabrication to those of large-area electronics on rigid substrates [13]. While all these manufacturing techniques are effective at creating fully functional stretchable and/or flexible electronics, they are complex, require prolonged fabrication time and dedicated facilities and infrastructure. Use of cost-effective additive manufacturing processes enables a simple yet effective manufacturing method for stretchable electronics making it more accessible and user-friendly.

1.2.1 Additive manufacturing methods

The ability of individuals to realize complex parts, molds, and even circuit boards without requiring enterprise scale facilities is enhanced by the easy availability of personal computers, open-source 3D design software tools, and hobby-oriented CNC mills. However etched circuit boards are inelegant, planar objects requiring soldering and cabling, and integrating these into more aesthetically elegant curved devices is difficult at

best. This can be overcome through freeform fabrication systems capable of producing electronics and structures together [10].

Additive Manufacturing technologies have expanded vastly over the past 2 decades. While originally considered apt for rapid prototyping (RP), the advent of new materials and processes has contributed to an incredibly vast array of applications. In recent years 3D printing has risen rapidly to the foreground as a contender for a very competitive process in terms of cost and speed. From industrial size printing machines to desktop printers, 3D printing is quickly gaining popularity. With the larger selection of materials available today, as well as the wide variety of post treatment procedures, the scope for this technology is growing quickly – far beyond the original idea of generating design iterations or inexpensive metal parts directly from a CAD file [26].

3D printing has its roots in ink-jet printing technology, of which there are two methods:

1. Continuous ink jet printing (continuous deposition) uses a stream of charged droplets and deflects those, which are to be used for printing.
2. Drop-on-demand (DoD) ink jet printing positions the ink jet printing head over the place where printing is to occur before depositing a droplet.

In 3D printing, the printer head serves to eject either droplets of binder or of liquid-to-solid compound to form a layer of an RP model. The ejection of droplets of the actual building material (liquid-to-solid compound) in DoD mode is known as drop-on-drop deposition, while the shooting of droplets of binder on the powder material is called drop-on-powder, or drop-on-bed (DoB) deposition [26].

Applications

Additive fabrication and RP technologies are mostly associated with applications in the product development and the design process as well as with small batch manufacturing. The comparatively high speed and low operational cost of 3D printers means that a large number of models can be produced during the product development phase. This makes it particularly cost-effective for applications in design either for studying function and form, creating proof-of-concept models or assisting in market research.

Thanks to its relatively high speed of manufacturing and flexibility, additive manufacturing is increasingly employed in non-manufacturing applications. With a focus on development of additive manufacturing technologies tailored to the needs of medicine and healthcare, RP processes are widely used in a range of medical applications, be it fabrication of custom implants and precise 3D printed organ models or creation of complex scaffolds for tissue engineering. The medical applications of 3D printing can be categorized as follows [27]:

- Bio-modelling: Fabrication of physical models of human anatomical parts and biological structures for surgical planning
- Custom implants: Design and fabrication of patient-specific implants for prosthetic operations, plastic surgery or rehabilitation
- Tissue engineering: creation of 3D printed scaffolds of varied materials is used in the preparation of contiguous tissue from cell cultures.
- Manufacture of micro-scale medical devices for drug delivery

Data for creating these 3D models is normally obtained through imaging using CT and MRI technology. This makes it especially convenient to tailor the creation of implants and models to match the needs of the specific patient. Cross-sectional slice data is generated with the ability to differentiate densities for various tissue regions, be it dense bony tissue or softer tissue regions. These contours are then interpolated to form a full 3D image [28, 29, 30, 31]. These medical models have a multitude of applications:

- To aid production of a surgical implant
- To improve surgical planning
- To act as an orienting aid during surgery
- To enhance diagnostic quality
- To be useful in preoperative simulation
- To achieve patient’s agreement prior to surgery
- To prepare a template for resection

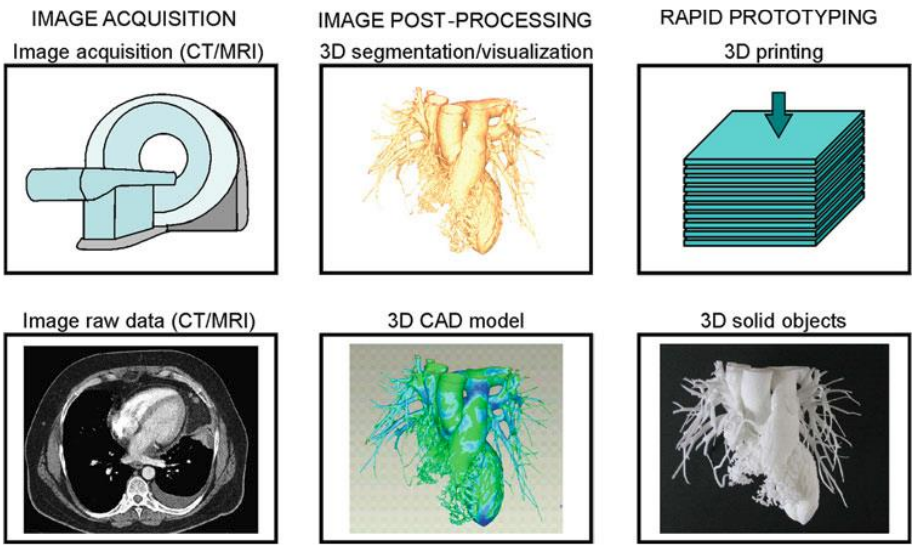

Figure 8: Three major steps in the process chain: image acquisition, image post-processing and rapid prototyping. Images are acquired using CT or MRI. Image raw data then transferred to dedicated post-processing workstation. 3D segmentation and visualization are performed and CAD model of the segmented structures can be generated. Such data can then be used by rapid prototyping machines to create the 3D solid object by addition of material layers [31].

Some key issues that hinder the wide-spread application of these methods for developing medical models are [28]:

- Speed: Since preparing medical data models is time consuming it is not suitable for emergency surgical procedures
- Cost: It is difficult to quantify the benefits from use of 3D printing in medical applications in comparison with the costs of acquiring and operating such devices.
- Accuracy: Matching accuracy of current RP processes to medical requirements is an area for improvement: the range of application of 3D printing is quite large and the resolution might not be tailored to the needs of the particular application.
- Materials: Due to the nature of applications, there is a need for bio-compatible material that can be used in RP processes.
- Ease of Use: high degree of expertise is required to achieve complex, high precision models. Significant training in data preparation and printing is necessary for efficient use of RP techniques.

An emerging area in the use of RP processes is in 3D tissue engineering and computer-aided organ printing. Tissue engineering relies on fabrication of an implantable vitalized organ-like tissue. The cells require a scaffold with interconnected pores that guide them in that volume during their growth. The internal 3D structure is hence essential for cell ingrowth and vascularization. Such scaffolds determine the bio-functional architecture of the growing tissue. 3D printing allows for highly precise and customized scaffold architectures to fit into the tissue defect of an individual patient as compared to traditional techniques such as molding and casting [32].

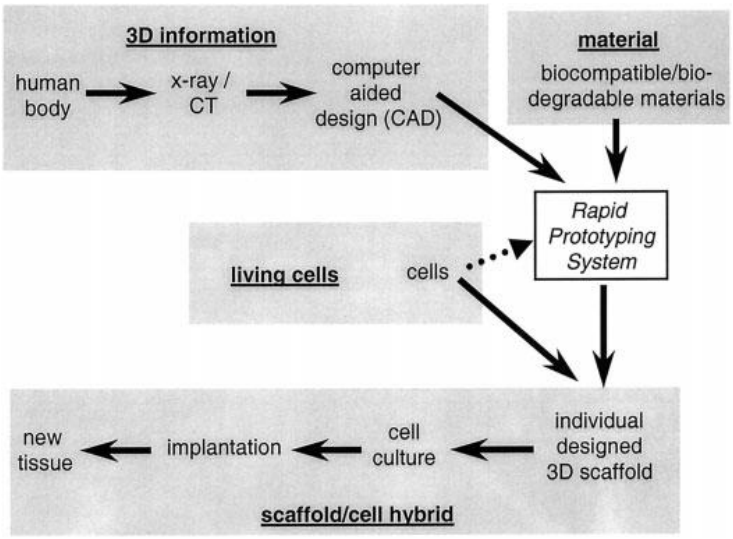

Figure 9: Concept of the fabrication of individual scaffold/cell hybrids by the combination of rapid-prototyping and tissue-engineering techniques [32].

While tissue engineering technology has tremendous applications in solving an organ transplantation crisis, assembly of vascularized 3D soft organs remains a big challenge. This is however possible to achieve through 3D organ printing via computer-aided, jet-based 3D tissue-engineering of living human organs. Organ printing involves three sequential steps: pre-processing (data preparation and analysis for specific organ); processing (actual organ printing process); and post-processing (organ conditioning and accelerated organ maturation and compatibility with host). Mironov et al., developed a cell printer that can print gels, single cells and cell aggregates [33]. Figure 10 below shows images of printed cells and tissue constructs.

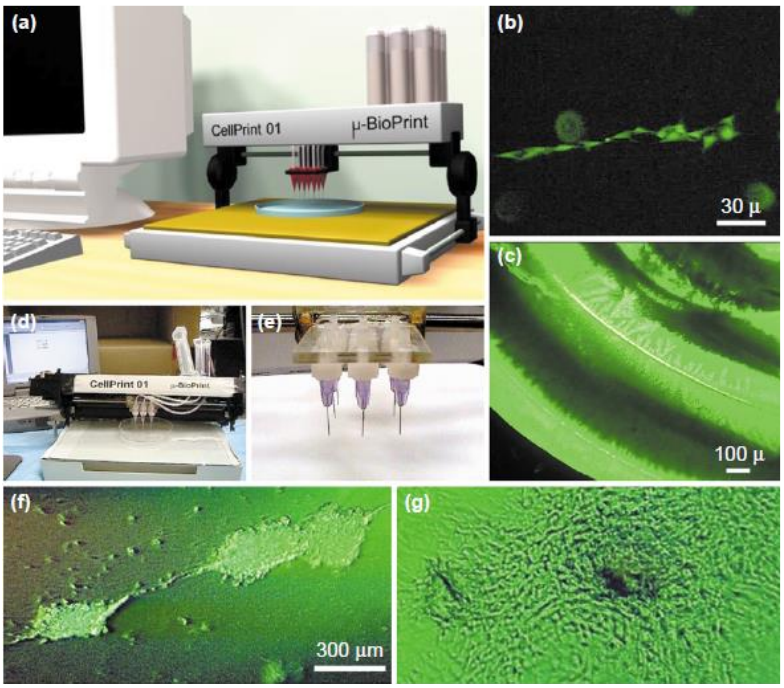

Figure 10: Cell printer and images of printed cells and tissue constructs. (a) Cell printer. (b) Bovine aortic endothelial cells printed in 50-micron size drops in a line. (c) Cross-section of the p(NIPA-co-DMAEA) gel showing the thickness of each sequentially placed layer. (d) Print head with nine nozzles. (e) The printer nozzle X, Y, and Z coordinates to print a dot are transmitted to the printer, which is controlled by a Microchip PIC 16F877. Endothelial cell aggregates 'printed' on collagen before (f) and after their fusion (g) [33].

A step further in this regard is the ability to three-dimensionally interweave biological tissue and structural materials with functional electronics which could enable the creation of bionic organs with enhanced functionalities as compared to regular human organs. Mannoor et al. developed a method for additive manufacturing of biological cells with structural and nanoparticle derived electronic elements. A bionic ear (shown in Figure 11) generated via 3D printing of a cell-seeded hydrogel matrix with an intertwined conducting polymer consisting of infused silver nanoparticles, with in vitro culturing of cartilage tissue around an inductive coil antenna, exhibited enhanced auditory sensing for radio frequency reception suggesting a means to intricately merge biologic and nanoelectronic functionalities via 3D printing [11].

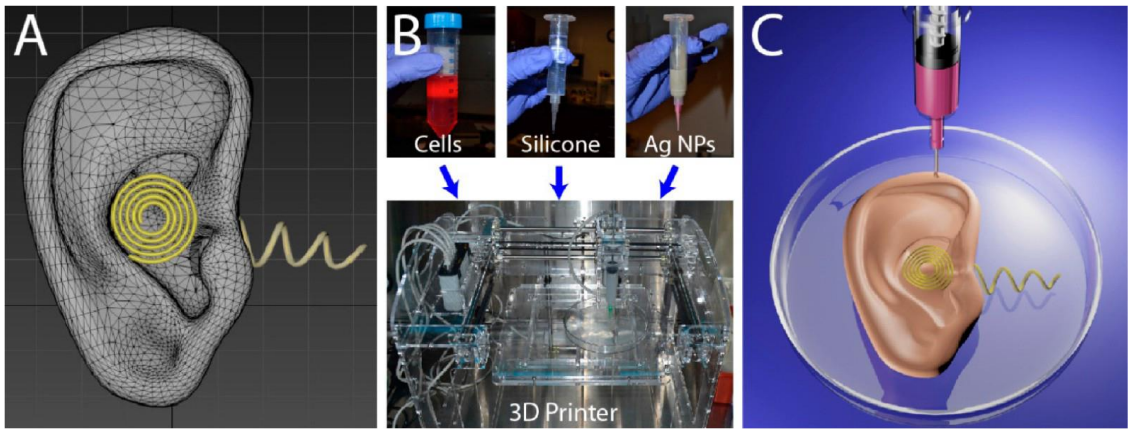

Figure 11: 3D interweaving of biology and electronics via additive manufacturing to generate a bionic ear. (A) CAD drawing of the bionic ear. (B) (Top) the functional materials: biological (chondrocytes), structural (silicone), and electronic (AgNP-infused silicone) used to form the bionic ear. (Bottom) Fab@home Model1 3D printer used for the printing process. (C) Illustration of the 3D printed bionic ear [11].

1.2.2 Material selection & curing methods

Silicone is a biocompatible, flexible material whose composition can be altered as needed to attain required structural and geometrical properties, which makes it an ideal substrate and structural material for 3D printing stretchable electronics. Silicone elastomers can be cross-linked ("cured" or "vulcanized") into solid forms through a variety of cure systems. The most common curing systems are:

1. Addition cure chemistry (platinum catalyst) which does not require moisture or open air, and
2. Condensation cure (tin catalyst) chemistry which requires airborne moisture.

Dual cure systems also exist, which are formulated to react with both ultraviolet light and humidity (water vapor in the air). Dual cure systems are especially useful with complex shapes as when exposed to UV light (of the appropriate wave length and intensity), it cures rapidly (seconds) to produce a durable and flexible optically clear, non-yellowing and chemically resistant sealant, adhesive or coating. Silicones also exhibit excellent electrical insulation properties. The moisture cure portion of the dual cure feature ensures that all of the material cures where UV exposure is difficult or imperfect. Pure RTV (Room Temperature Vulcanization) cures can usually be accomplished within 24 hours at ambient temperatures or faster at elevated temperatures.

Silicone elastomers have many properties that make them well suited for applications in the healthcare industry. These materials feature biocompatibility, strong heat aging properties, high chemical resistance, ultraviolet (UV) stability, low compression set, purity, clarity, ease of processing, and stable mechanical properties at a temperature range from –40°C to 200°C.

New methods have been developed to accelerate curing of liquid silicone rubber (LSR) by UV light where the crosslinking is initiated by a photochemical reaction rather than heat. This allows silicone rubbers to be combined with many temperature-sensitive materials. Such co-extrusion is not possible with traditional thermally cured silicone elastomers.

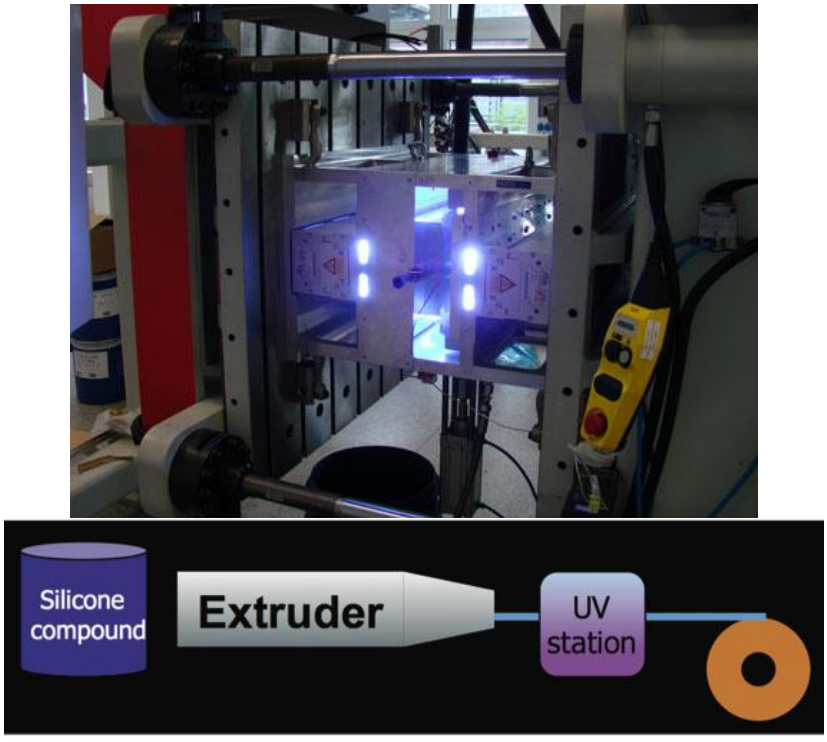

Figure 12: UV LSR molding during UV curing (top) [34] and a schematic of extruder head with UV curing module

Like heat-curing LSRs, UV-curing LSR is based on an addition cure mechanism. The major difference is that UV-curing LSR contains a photosensitive catalyst. UV-cured silicone elastomer typically retains the same properties and benefits of thermally cured silicone elastomers. UV-curing LSR typically cures quickly at ambient or slightly

elevated temperatures (25–40°C). Thicker parts, in particular, may vulcanize much more quickly with the UV-curing technology than with thermal curing technology because the low thermal conductivity of the silicone rubber is no longer a limiting factor. Another advantage of UV curing is the fact that the crosslinking reaction begins when the light is switched on rather than when the liquid rubber has been extruded, virtually eliminating the issue of silicone rubber scorching. As the cure is initiated through UV radiation, the degree of cure from outer surface to the core of the three-dimensional product is uniform, which allows high-speed extrusion of thick wall tubing and profile free from common defects such as internal porosity with UV exposure time required for cure being as short as 0.5 seconds, allowing extrusion of silicone at much higher rates compared to existing thermal curing systems. It is also possible to interlace UV curable color inks with printable electronics. UV curable insulating inks have a low solvent chemical content, so are less likely to damage any sensitive printed electronics.

Outgassing:

Silicone rubbers are made of three basic components: polymers, reinforcing fillers and additives. The basic structure of the polymer is a silicon-oxygen bond – the same bond that forms the basis of quartz or glass. Liquid silicone rubbers are available as two-component systems: the A component contains added platinum catalyst; the B component contains a methyl hydrogen siloxane acting as a cross-linking agent and a high-molecular alcohol as inhibitor. Curing is effected by way of a platinum-catalyzed hydrosilylation reaction in which the methyl hydrogen siloxanes add to the vinyl groups of the polymer. The reactivity is controlled via the catalyst and inhibitor concentrations. The outgassing process of silicone rubber is based on a diffusion mechanism [35]. The rate of outgassing can be reduced through heat treatment which can be utilized to both increase the speed of curing of extruded silicone as well as limit/slow the rate of outgassing upon deposition.

Chapter 2

Design and development

2.1 Overview

This work focuses on designing and testing the feasibility of an integrated additive manufacturing method for printing stretchable electronics. One of the primary objectives of the study is to select the right conductive and non-conductive materials – either custom-developed or off-the-shelf. These must fit the requirements, both electrical (the conductive material must provide effective conductive pathways) and mechanical (both the conductive and non-conductive materials must withstand the forces and strain due to stretching and flexing of the device) properties while being able to be deposited via an additive manufacturing process. As discussed in the literature review a number of materials have been researched and found to be useful for such applications. However we have also taken into consideration the constraints imposed on material selection due to the nature of the additive manufacturing process. These constraints, other requirements and parameters evaluated during material selection, design and development of a custom extrusion head to accommodate the properties of the materials selected and the control methods are discussed in the following sections.

2.2 Silicone selection

2.2.1 Non-conductive silicone

As discussed before, silicone has many favorable characteristics that make it ideal as a material for flexible electronics. While polyurethane-based substrates or plastic flexible substrates have been employed in certain applications, silicone provides a better solution for the current study due to its biocompatibility, ease of extrusion, easy availability and cost-effectiveness. With the consideration that a silicone polymer would be used for the conductive material, it is convenient and more compatible to use a silicone material for the structural build as well.

Some of the key parameters that were evaluated while researching non-conductive silicones were:

- Curing method and compatibility with optoelectronic components
- Single cure v/s dual cure: standalone UV cure / UV + moisture cure
- Curing speed (skin-over time, tack-free time, etc.)
- Extrusion rate and viscosity
- Chemical composition
- Material consistency and appearance
- Mechanical strength

Loctite (by Henkel Industries) manufactures a number of UV cured silicones. Loctite also makes custom UV curing modules as required for the application. Of these silicones 2 main types of silicones were explored: namely acetoxy and alkoxy cure mechanisms. Acetoxy-based silicones are corrosive and are primarily used in industrial applications where as alkoxy type silicones are non-corrosive and used mostly in electronics applications. Considering that the structural silicone will be interacting with electronic components in the build of stretchable circuits, alkoxy-type silicone proves to be the ideal structural material.

Koba UVG is another promising material type slowly gaining popularity with UV cured extrusion systems for 3D printing. Many new desktop and medium-scale industrial 3D printing systems use this material for its ease and speed of cure, as it usually sets in seconds and provides good structural support. It is tested to withstand only up to 15% elongation.

While thinning of higher viscosity silicones does provide for easier extrusion, the outgassing process, both immediately upon deposition and through the curing period, can interfere with the chemical composition of any conductive material deposited on additional layers. With this in mind thinning of silicones was ruled out and only lower viscosity silicones were considered in the material selection process. Specifically the Loctite Nuva-Sil 5084 and Loctite 5240 were sourced. The complete matrix of non-conductive silicones that were shortlisted is discussed in detail in Figure 13.

2.2.2 Conductive silicone

The primary requirement of a conductive material for printing stretchable circuits is the ability to form reliable pathways of comparatively high conductivity, robust traces capable of withstanding uni-axial or bi-axial strain, without being prohibitively expensive or hazardous to use. Considering that many off-the-shelf electrical repair sealants and adhesives match these properties these make a good starting point for conductive material selection.

Conductive sealants/adhesives were considered from 3 main sources: Silicone Solutions, OH, Henkel Adhesives (under the Loctite brand of conductive silicones) and MMS-EC (Moreau marketing & Sales), PA. Some of the promising materials among those researched included:

- MMS-030 – silver coated glass EC RTV silicone
- MMS 080 – pure silver EC RTV silicone (grittier composition)
- Loctite 4298 – thermal cure with 11% stretchability
- Loctite 5421 – RTV with 40% stretchability and conductivity of 0.01 S/cm
- SS-261/26F/26S – Moisture-accelerated RTV

While both Loctite and MMS-EC silicones cured favorably, they displayed lower stretchability as compared to the ones from Silicone Solutions. The behavior of the SS-26 family of silicone materials in similar applications was also better documented as it has been used as a conductive material in the print of bionic organs by both Lipson et al. and Mannoor et al. in comparable manufacturing methods [10, 11]. However while the SS-26F exhibits favorable conductivity it has a higher hardness and flows more readily upon deposition as compared to the structural silicones selected. Figure 14 shows additional details of the silicones considered.

From preliminary calculations it was estimated that a trace width of 0.25mm - 0.5mm will be required (analogous to size of electrical etched traces on PCBs) with a favorable bead size of 0.25 x 0.5mm (rectangular cross-section). With a suitable viscosity, the SS-26S provides the right extrusion properties for a syringe-based robocasting process considering that higher gauge needles will need to be employed to achieve deposition sizes mentioned above. The SS-26S uses silver filler to infuse conductivity with nanoparticles. As seen before, the use of nanoparticles provides numerous advantages and hence the SS-26S was selected as the conductive material. While Silicone Solutions does make customized SS-26S with required size nanoparticle filler, the current study uses the standard off-the-shelf SS-26S with a particle size of 14 microns, considering cost and time constraints in lieu of additional testing required to determine appropriate nanoparticle size in the filler. Though the standard SS-26S does suffice for the scope of this project, further studies with this material can certainly incorporate varied nanoparticle configurations to study its effect on the electrical conductivity of the material and hence optimize the size and quantity of material deposition required in the printing of conductive traces.

Figure 13: Non-conductive silicone material selection matrix

		Material properties (uncured)						Curing					Cured material	
Silicone	**Mfg.**	**Stretchability***	**Chemical type**	**Appearance**	**Extrusion rate (g/min)**	**Viscosity (cP)**	**Material type**	**Cure type**	**Skin-over time (s)**	**Irradiation source**	**Irradiation power (mW/cm2)**	**Tack-free time(s)**	**Strength (N/mm2)**	**Shore Hardness (Durometer A)**
Loctite 5084 Nuva-Sil	Henkel Electronics	250	Alkoxy - non-corrosive	Transluscent straw colored paste	140 - 300 [0.63 Mpa - 15s @ 25deg C]	-	Thixotropic (Reduced migration of liquid product)	UV + moisture	2		250	4	High (>3.4)	32-47
											75	6		
Loctite 5092 Nuva-sil	Henkel Electronics	75	Alkoxy - non-corrosive	Yellow-to-green liquid	-	4000 to 7500	Self-leveling (uniform cavity fill)	UV + moisture	300 min	Electrodeless D	250	75-90	Medium (>0.6)	32-50
											75	270-600		
										Electrodeless H Bulb	250	20-30		
											75	60-75		
										Zeta 7200	250	10-20.00		
											75	<90		
Loctite 5031 Nuva-sil	Henkel Industrial	60	Acetoxy dual cure	Light yellow transluscent liquid	-	4000 to 7500	Self-leveling (uniform cavity fill)	UV + moisture	<20 min		70	<20	Medium (>0.55)	28-40
Loctite 5033 Nuva-sil	Henkel Industrial	150	Acetoxy dual cure	Light yellow transluscent paste	100-170 [0.6 Mpa - 15s @ 25deg C]	-	Thixotropic (Reduced migration of liquid product)	UV + moisture	<15 min		70	<20	>2.75	45-65
Loctite 5039 Nuva-sil	Henkel Industrial	150	Acetoxy dual cure	Light yellow transluscent paste	150-320 [0.6 Mpa - 15s @ 25deg C]	-	Semi-flowable sealant	UV + moisture	<20 min		70	<20	>1.0	32-48
Loctite 5240	Henkel Industrial	250 - 450	Alkoxy - non-corrosive	Clear liquid w/ yellow-to-green tint	-	15000 to 35000	Thixotropic product that will thin with shear yet provides	UV + moisture		Zeta 7760	225	50-55	>3	>40
										Zeta 7411-	50	90-105		
										Zeta 7215	90	90-105		
										Electrodeless H Bulb	500	5 to 10		

* > % Elongation @ break

Figure 14: Conductive silicone material selection matrix

		Material properties (uncured)					Curing				Cured material	
Silicone	**Mfg.**	**Stretchability***	**Chemical type**	**Appearance**	**Viscosity (cP)**	**Material type**	**Cure**	**Tack-free time** (min)	**Working time** (min)	**at deg. C**	**Shore Hardness (Durometer A)**	**Conductivity (S/cm)**
SS 261	Silicone Solutions		Non-corrosive	Silver-Tan (Custom colors available upon request)	400000	Thixotropic paste	RTV (Accelerated moisture cure)	45	> 24 hrs	115	70	200
SS-26	Silicone Solutions		Non-corrosive	Silver-Tan (Custom colors available upon request)	30000 to 80000	Thixotropic paste	RTV (Accelerated moisture cure)	30	15	Room temp	70	200
SS 26S	Silicone Solutions	200	Non-corrosive	Silver-Tan (Custom colors available upon request)	500000	Thixotropic paste	RTV (Accelerated moisture cure)	30	15	Room temp	50	200

* > % Elongation @ break

2.3 Extrusion head design

2.3.1 Syringe and Nozzle selection

In order to extrude heavy thixotropic pastes with uniform deposition characteristics, the robocasting process proves ideal. This method employs a robotic syringe extrusion system with the bead size controlled by the nozzle selection, extrusion speed, and printing speed.

For achieving a rectangular cross-section of 0.25 x 0.5 mm^2 (to ideally match planar traces like on a PCB) rectangular cross-sectional needles were considered. However such needles are more expensive compared to regular circular nozzles which are more readily available. A circular cross-section of > 0.25mm^2 and < 0.5mm^2 would suffice in the current application. Some key parameters in selection of needle size:

- Needle type & material: steel shaft in plastic hub/ all-plastic design/ glass hubs
- Needle gauge: higher gauge needles provide smaller cross-section, but cause issues like clogging due to the nature of the material used.
- Fixturing to syringe: Luer-lok, Luer slip or integrated nozzles.
- Blunt v/s hypodermic needles
- needle lengths – Short needles(1/2in) v/s longer shafts (1-1/2in)
- Shaft wall thickness – Thin-walled v/s thick-walled needle

While extrusion based desktop 3D printing systems like Fab@home and some RepRaps use conical plastic nozzles, they are not available in the sizes required for the current application. Luer-lok needles come in a vast range of sizes and provide easy use and good strength due the type of attachment to the syringe barrel. This also makes it easy to shift to different deposition sizes with a single loading of the syringe with a particular material type, providing higher flexibility in the manufacturing process. For the purpose of the preliminary studies inexpensive plastic syringes were used.

Figure 15 below shows a preliminary test of extrusion characteristics with a 1ml syringe with attached Luer-lok needle. The 1ml barrel was considered keeping in mind the

volume of conductive material required to be extruded in general applications (using larger quantities might cause complications since the conductive silicone has a moisture-accelerated RTV cure with low skin-over times, and can cure within the syringe before the entire extrusion process is completed, especially for longer prints). Corn syrup was chosen as the test material to examine extrusion from the syringe since its consistency and viscosity was comparable to the conductive silicone selected and provided a cheap and easy-to-clean.

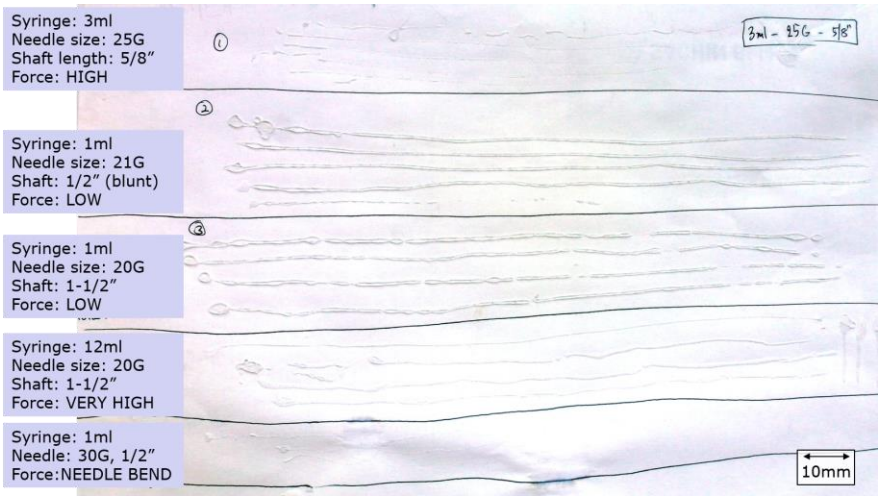

Figure 15: Different needle sizes were used to extrude corn syrup. Bead size and type and force required were documented to aid in needle selection

From preliminary estimation, an extrusion velocity in the range of 2-20 mm/s would be desired from the syringe nozzle. With this estimate, an empirical volume flow rate calculation was done assuming the conductive silicone displays non-compressible flow characteristics.

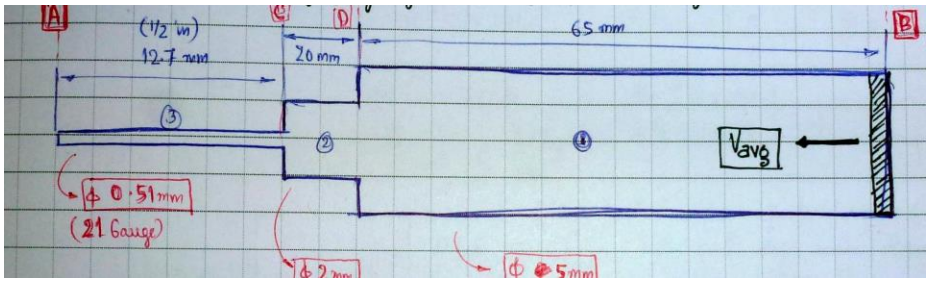

Figure 16: Volume flow rate calculations for syringe

From Figure 16 for a 21 gauge needle of ½" shaft:

Area at c/s A: $A_a = \pi D_a^2/4 = 2.04 \times 10^{-7}$ m^2

Area at c/s B: $A_b = \pi D_b^2/4 = 1.93 \times 10^{-5}$ m^2

Desired extrusion velocity, $V_a = 4$ mm/s $= 4 \times 10^{-3}$ m/s

Then Plunger velocity, $V_b = A_a V_a / A_b = 4.15 \times 10^{-5}$ m/s

Reynold's number, $R_e = \rho V_{avg} D/\mu$, where dynamic viscosity, $\mu = 500$ kg/ms (for the conductive silicone SS-26S), density, $\rho = 3060$ kg/m^3 and $V_{avg} = V_a$

Hence, Re $= 1.25 \times 10^{-5}$ (<2300 ⇨ Laminar flow)

Volume Flow rate (i.e. material extrusion rate): $\boldsymbol{V} = A_a V_a = 8.15 \times 10^{-10}$ m^3/s

Calculating pressure drops for all 3 zones (Figure 16) using Pouiselle's Law for flow through horizontal pipes [$V_{avg} = \Delta P D^2/32\mu L$], we get:

$\Delta P_1 = 1.72$ kPa

$\Delta P_2 = 20.40$ kPa

And $\Delta P_3 = 3.06$ MPa

Net pressure loss across syringe is $\Delta P_{net} = \Delta P_1 + \Delta P_2 + \Delta P_3 = 3.08$ MPa

Hence the push force required at the plunger is $F = \Delta P_{net} \times A = 59$ Newton

From these studies the 21 and 18 gauge needles were selected for the conductive material with 16 gauge needles opted for the structural silicone (the larger needle size also allows for faster deposition through increased flow rate).

2.3.2 Syringe tool design

To achieve the high levels of torque required to extrude the viscous paste from a low cross-section nozzle, several extruder designs were considered. In each case the extrusion was tested with the selected motor using a microcontroller (Arduino Uno) subroutine with bidirectional control to determine extrusion characteristics with a substitute material (corn syrup/ builder's silicone).

A linear actuator, L16 (Miniature linear motion series, Firgelli Technologies) was chosen for extrusion. This motor has a high peak power point of 175N at 4mm/s with a gear reduction of 150:1 with a maximum speed of 8mm/s. With its low weight and compact design, this motor suits the required application.

In order to design a mounting module for the syringe tool, a box-type design was selected with the syringe extrusion axis being parallel to the axis of the linear motor. Laser-cut acrylic sheets were used to assemble the box housing, using acrylic cement for assembly with no additional fasteners required for the box. This not only eliminated the need for fasteners in the main body construction and hence freed up volume to make a compact design, but also made it strong enough to withstand the forces exerted by the motor during extrusion. A V-channel was used to house the syringe. This helped to accommodate various syringe barrel sizes and enabled quick tool changes.

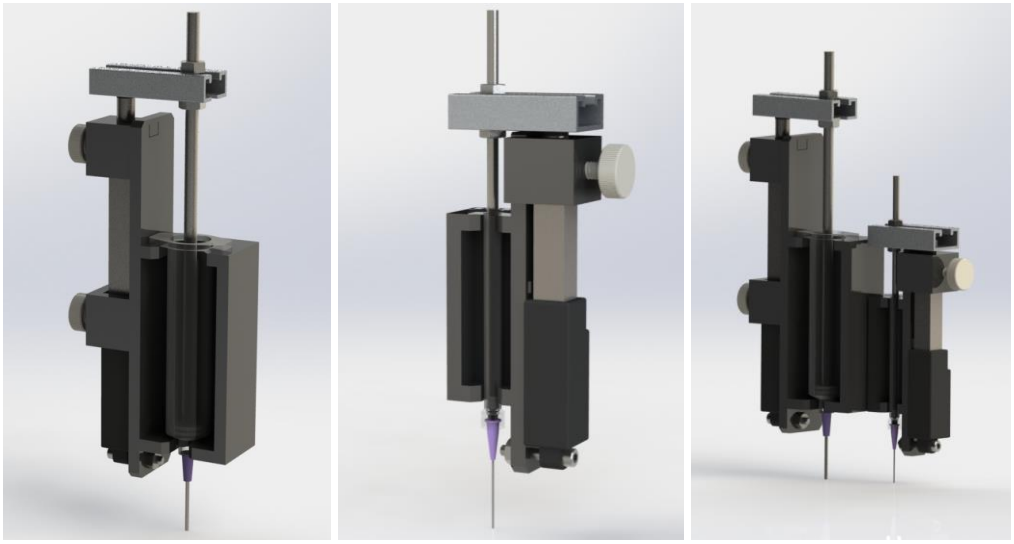

Figure 17: CAD modelling of syringe tool design (version 1) prior to build and testing. The 2 modules were designed so that they could be either used as standalone heads (for the 20ml and 1ml syringes respectively) or combined to mount as a single multiple-extrusion unit (rightmost)

While this design allowed for successful extrusion, the separation of axes of the motor shaft and the syringe affected the efficiency of extrusion. This was modified to apply force on the plunger of the syringe along the axis of the linear motor as shown in Figure

18. Pulse width modulation (PWM) was used to control motor speed and the motor was tuned to function at a good mid-range speed. One major drawback of this design is the length of the complete module. While a 50mm shaft suffices for the smaller motor (used on the 1ml syringe for conductive silicone) for complete travel of the plunger in the barrel, the larger 100mm shaft on the secondary motor (used for the 20 ml syringe) causes difficulties due to cantilevering when mounted on a robotic arm for 3d printing.

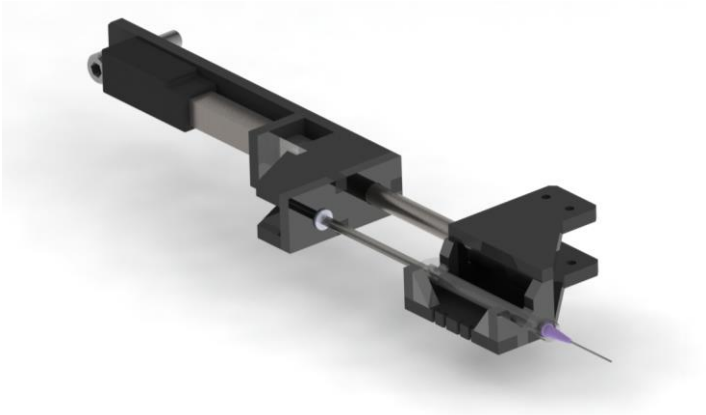

Figure 18: Same-axis linear actuation

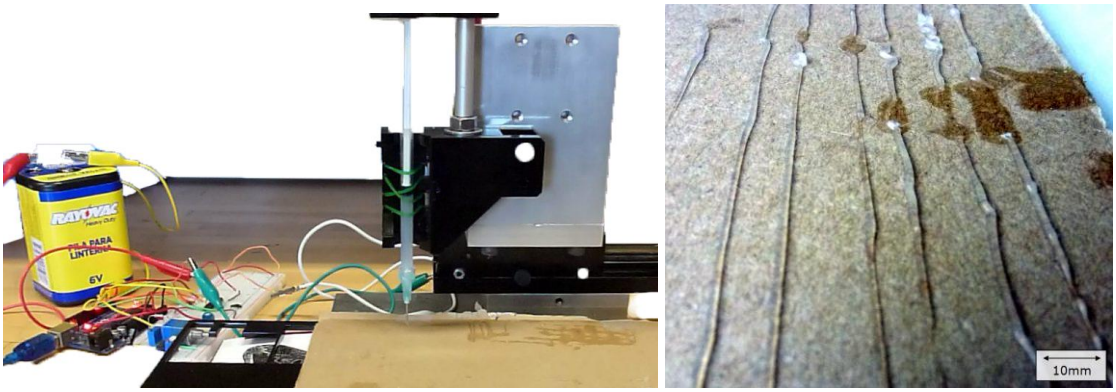

Figure 19: Extrusion setup with vertically mounted syringe tool using Arduino microcontroller with H-bridge used to control motor speed via PWM and (right) builder's silicone extruded from the linear motor in-axis syringe extrusion

An alternative method to achieve extrusion is to use a rotary motor. Figure 20 below shows an extrusion head design using a 3:1 gear reduction with spur gears translating the rotation of a 100:1 12V DC motor (Phidgets 3257E) with optical encoder (E4P US Digital encoder) to linear actuation with two 1/8th inch lead screws (32 pitch) which also

provide structural support to the motor housing platform. The whole setup is affixed with mounting plate for easy fixturing to a robotic arm.

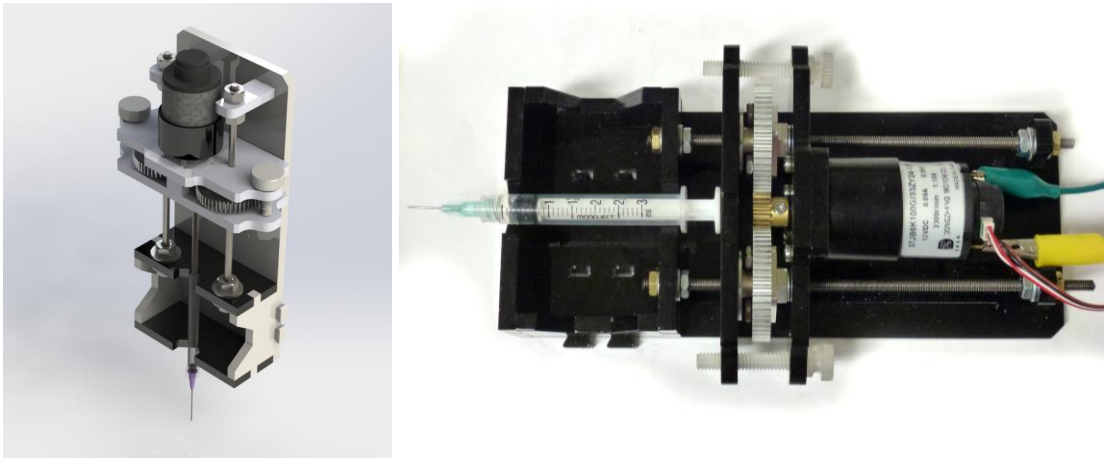

Figure 20: CAD model (left) and built prototype (right) of Custom Syringe extrusion head with 3:1 gear reduction using rotary DC motor with encoder incorporating velocity feedback control (concept courtesy Tim Zalusky)

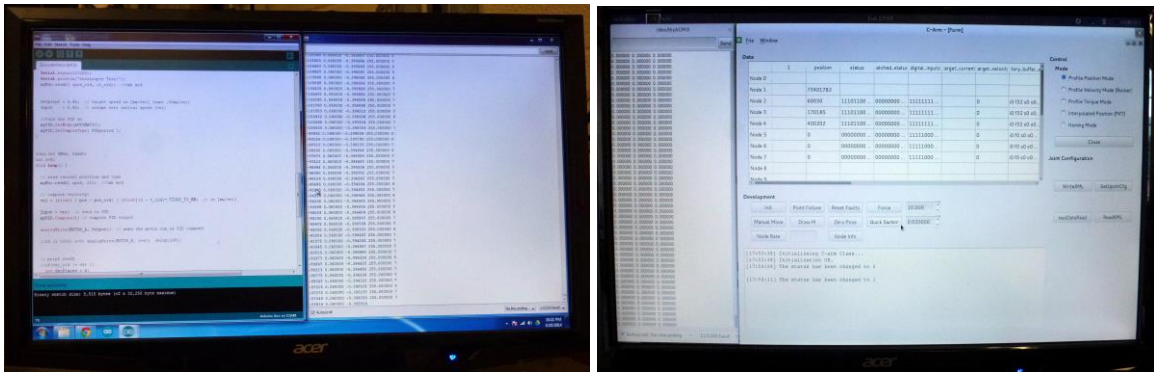

Figure 21: (left) Serial communication with Arduino @ 115200 baud rate via USB 2.0 (right) Trajectory control of Corvus robotic arm with mounted syringe tool

The Phidgets DC motor has good low end torque characteristic which is ideal for silicone extrusion as it requires low extrusion velocities with high force requirements. Initial tests with PWM controlled extrusion speed variation showed favorable results. In order to implement velocity feedback for steady state volume flow rate, PID control was implemented for the plunger velocity.

2.3.2 Extrusion method

A major challenge to extrusion-based additive manufacturing is controlling the start and stop of extrusion in-trajectory. Commercial 3D printers use a filament-based thermoplastic material which has the advantage that the molten material being deposited will remain so until cooled and show predictable extrusion characteristics. Thixotropic pastes like the SS-26 however have the disadvantage of having a complex rheology and have higher chances of clogging during extrusion due to agglomerate formation or drying of the paste at the nozzle tip.

Li et al. [36] developed an analytical process model for extrusion of such pastes and to regulate extrusion-on-demand. Closed-loop control methodology for this type of 3D printing is mostly concerned with either constant-velocity or constant-pressure based methods to ensure reliable steady-state flow. Robocasting and Fused Deposition Modeling (FDM) use position-controlled methods to advance the plunger at a constant velocity to achieve a steady paste flow-rate. Robocasting differs from FDM in that instead of a thermoplastic material, a colloidal gel is extruded and it rapidly solidifies upon deposition through various curing methods. In a position-controlled method extrusion-on-demand is achieved by retracting the filament or syringe plunger by a predetermined displacement. Constant velocity methods however are useful for applications that are interested only in the steady-state velocities. Constant pressure methods are also sometimes employed for the same effect through the use of pressure regulators with internal control logic, however for the current study a velocity feedback method provides for easier implementation. Some key criteria to be considered for this type of control are:

- Regulating the steady-state extrusion speed for the extruder.
- Starting and stopping extrusion-on-demand in-trajectory.

Closed-loop Velocity control:

Deuser et al. developed a control method for Freeze-Form Extrusion Fabrication for Functionally Graded Material Parts [37]. In this study we employ a similar control

methodology for paste extrusion that utilizes an extrusion velocity controller. Our plunger velocity was controlled via PID control to ensure a steady extrusion flow rate. Extrusion speed could be set either in manual mode or in conjunction with the extrusion-on-demand process while printing on a layer trajectory by Corvus.

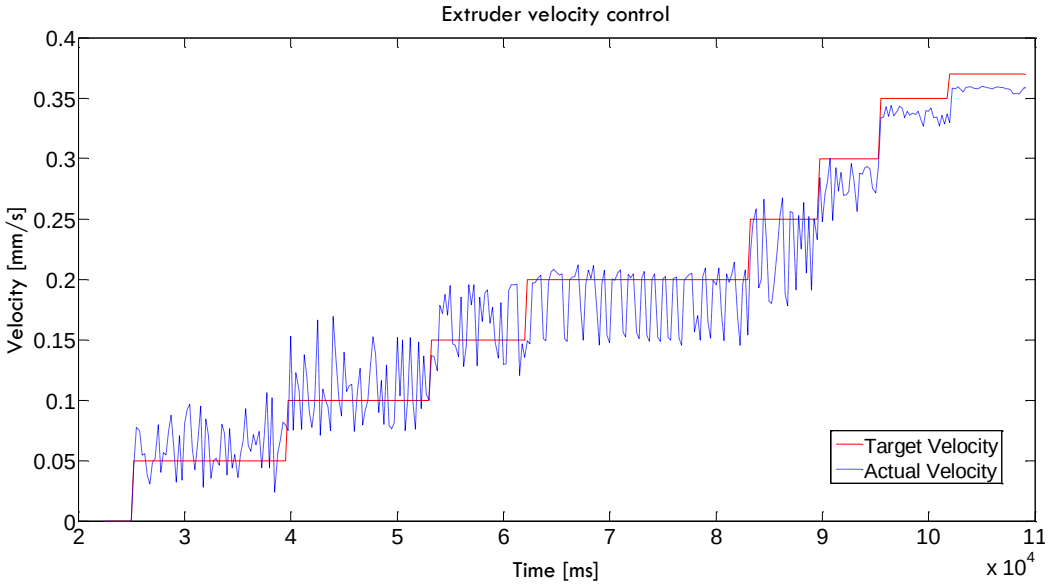

Figure 22: A PID control method is applied to control the extrusion velocity for the syringe. Here the actual plunger velocity is plotted against the target speed entered by user via serial input

Printing parameters:

Some key parameters to define for control of the extrusion process are:

- Syringe tool trajectory speed
- Pen-up and pen-down (approach and retraction of needle from work surface)
- Free travel speed of extrusion head (in no-printing tool path)
- Height of pen-up and pen-down operations: this can be fine-tuned to prevent agglomeration of paste at the end of the printing trajectory
- Motor start time (in relation to start of printing trajectory) and
- Motor stop time (at the end of the printing)

Chapter 3

Experiments & Results

3.1 Overview

The purpose of these experiments was to (a) determine the feasibility of using an additive manufacturing method to print stretchable electronics using conductive silicone, (b) to determine and fine-tune various printing parameters, and (c) study material properties and their effect on the manufacturing process. The purpose of this approach would be to implement and document a reliable technique to print stretchable electronics by:

1) Testing the extrusion and cure behavior of conductive silicone SS-26S on flexible substrates with an extrusion-based manufacturing process as this information is currently unavailable. This information can assist in fine-tuning the extrusion head design, syringe and nozzle selection and selecting the printing parameters.
2) Understanding the electrical behavior of the conductive silicone and its effect on the functioning of the printed circuits. The primary application of SS-26S being as an electrically conductive sealant, its behavior with respect to printed stretchable electronics is unknown. While this material has been successfully used previously

to create reliable conductive pathways in 3D-printed rigid structures and in bionic organs, its conductive performance under strain has not been previously tested.

3) Determining feasibility of integrating structural and conductive silicone layers to form fully integrated stretchable functional device. By studying the interfacing between the two silicones, the material selection can be optimized for future applications.
4) Studying different interfacing methods for conductive silicone with optoelectronic components to achieve optimal connectivity and sustain applied strains without breaking contact.

Our literature review in this area showed a number of promising methods that we could adopt for achieving stretchable circuits with the SS-26S. One way to achieve good stretchability is to effectively isolate the rigid and flexible components of the circuit (the electronic components and the stretchable conductive silicone traces respectively) by creating pockets of surface mount (SMT) components interconnected with long sweeping interconnects. However there is no data available on either the methods or results of effect of strain on circuits created from conductive silicone interconnects. Considering that we are using a substrate of comparable flexibility (40 durometer Shore A hardness) as the conductive silicone, there is an opportunity to test the effect of strain on the rigid electrical components of the embedded circuit, as well as the metal-to-silicone bonding at the interfaces of the components and the conductive traces.

The gap in the literature underscores the lack of information in this area to establish the feasibility of this approach. This lack necessitates a sequence of experimental verification steps to determine whether this extrusion-based 3D printing approach using conductive silicone interconnects is feasible and whether it can be successfully applied in the manufacturing of bio-integrated devices which need biocompatible circuitry with good stretchability characteristics. To this end, a sequence of experiments was conducted to test the following hypotheses:

3.2 Hypotheses

1. It is possible to extrude conductive silicone using a syringe-based robocasting process to print conductive traces for circuitry with integrated optoelectronic components, with options for quick tool changes and fine deposition control.
2. The SS-26S silicone exhibits favorable conductivity for printing of stretchable circuits and maintains good conductive performance under uni-axial strain
3. It is possible to print complete fully-functional circuits with the defined manufacturing process and the printed circuits function electronically both with stretching and flexing of the embedded circuit 'skin'.

The sections below describe the experimental conditions, equipment, data collection, analysis and results used to test each of the hypotheses above.

3.2.1 Experiment 1: Extrusion and Cure of Silicone conductive ink

Extrusion control

For printing with CORVUS, a Trajectory-Based Start and Stop Method was employed to control extrusion. The trajectory-based method issues a "start" or "stop" command via serial input to the extruder before the desired start or stop point.

This method was tested for start commands by initiating extrusion from 500ms before the initial segment point was reached with a 2-speed pen-down and for stop commands by stopping the motor to end the plunger from 100ms before the final segment point was reached with a similar 2-speed pen-up travel to break off bead formation at the end of the extrusion. These delays account for the slow transient response for starting and stopping extrusion from application of force on plunger to actual extrusion of material from the needle end, due to the nature of the paste and the type of syringe used. Following this command, the extrusion velocity controller activates and sets the reference extrusion velocity to a predetermined value. Actual velocity is tracked via feedback loop and constantly compared to match the input speed with adequate PWM of the motor. The trajectory-based stop can produce a constant extrusion track width with no excessive

build-up. Approximately 20 to 40ms is required to stop extrusion. Longer delay times cause the extrudate track to stop short before the end of the segment, whereas shorter delay times cause build-up at the end of the segments as can be seen in Figure 23.

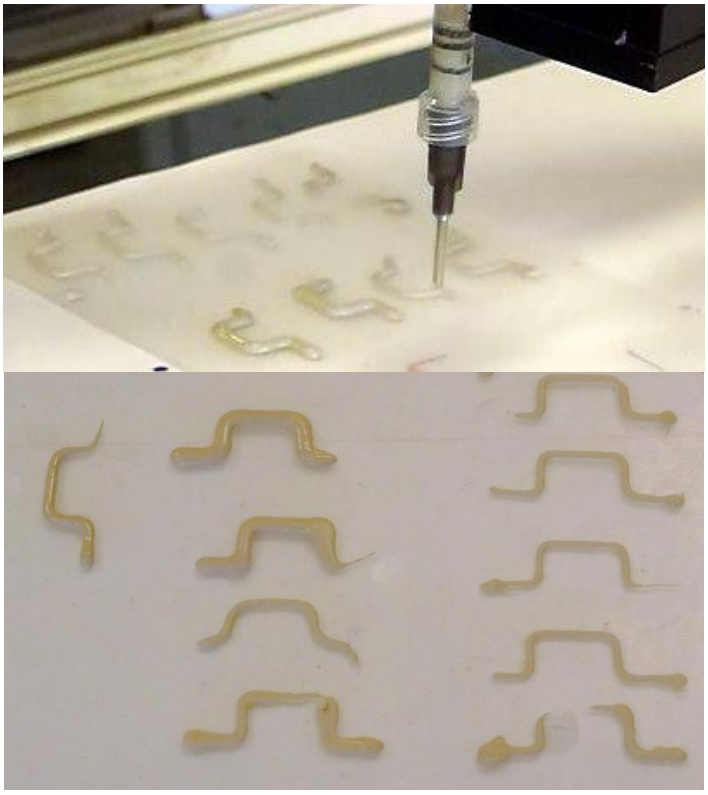

Figure 23: Extrusion segment deposition with combinations of various extrusion and travel speeds (bottom) and the extrusion using a 1ml syringe with various needles on a silicone substrate placed on the CORVUS worktable (top)

Experimental setup

The custom-developed syringe tool using high torque DC motor and high gear reduction module was specifically modified to mount on to CORVUS (Figure 24). CORVUS is a six-axis robot available at the Medical Robotics & Devices laboratory at the University of Minnesota and being developed at present by John O'Neill, PhD candidate. Three of the six axes of the robot arm were utilized to 3D print with the extruder head.

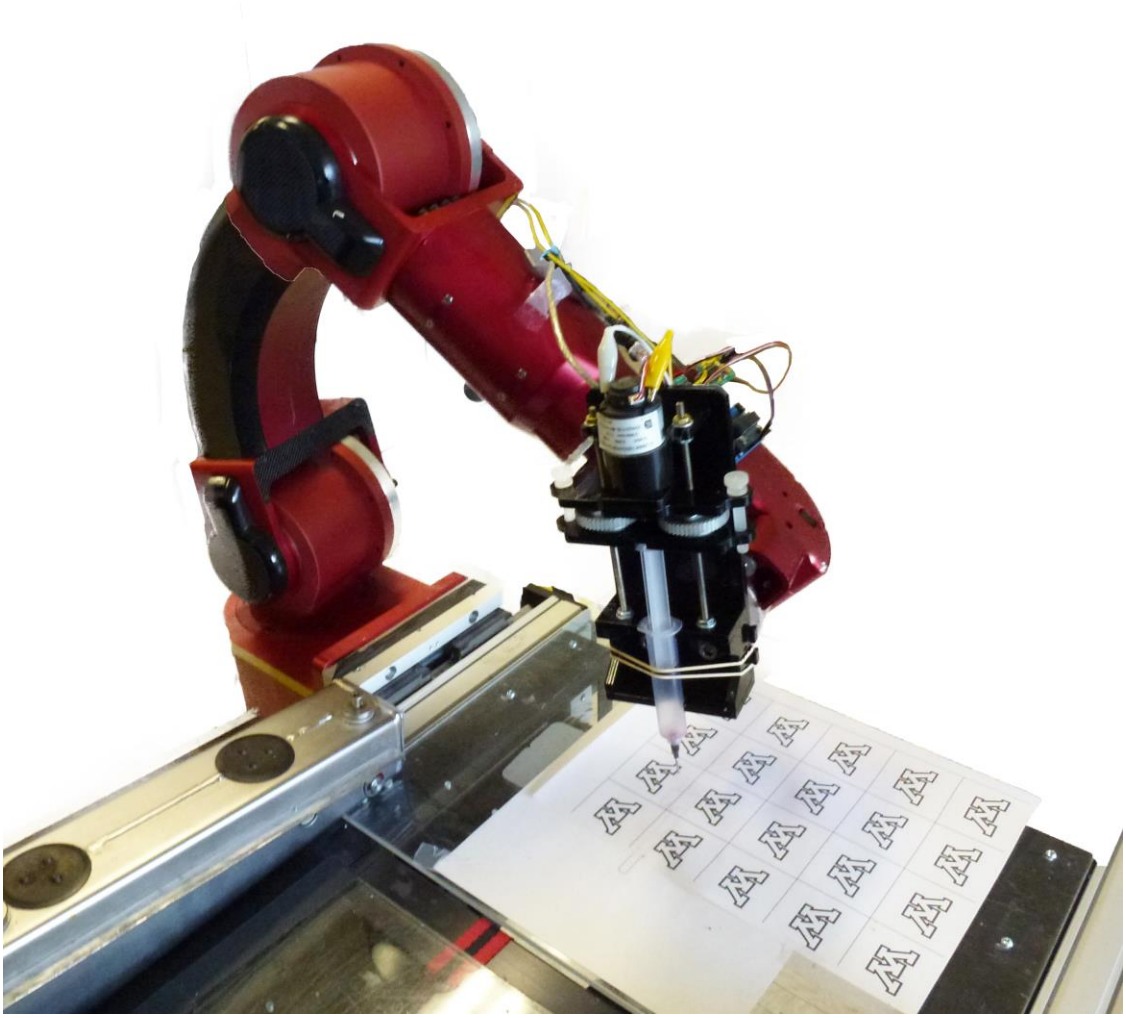

Figure 24: The syringe tool along with the Arduino module is compactly attached to the robot arm of CORVUS [12]. The worktable is stationary. The arm has 3 aces of motion controlled by the first 3 joints.

The robot arm was tested for position-based trajectory control using a custom Graphic User Interface (GUI) (Figure 26). Initial testing was done for free arm travel with extruder head to determine travel speeds for printing application as well as to overcome jerk in the motion of the arm. Then, tool paths for printing the conductive material for each layer were created using Inkscape (Figure 25) and sourced by the CORVUS trajectory program as a scalable vector graphic (.svg) file.

3 Set points were input through the CORVUS trajectory and extrusion control panel GUI to determine the plane of the work surface (Silicone substrate). This was then used as the

XY plane for the specific layer of the print with the tool path imported from the loaded trajectory .svg file, with successive layers defined by incremental Z values.

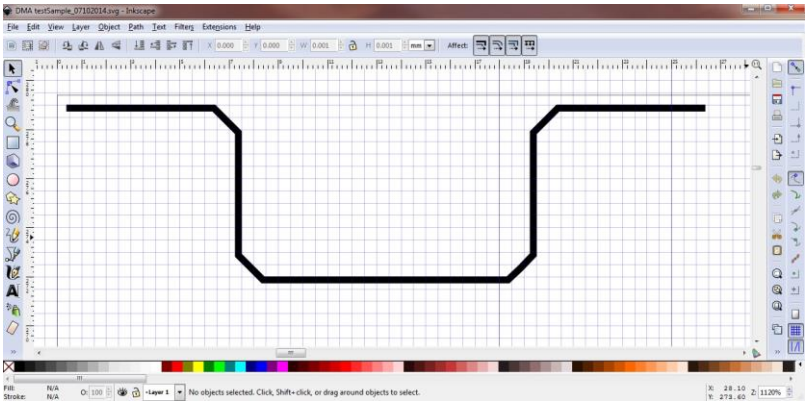

Figure 25: Tool path for printing defined as a .svg file corresponding to XY coordinates of worktable.

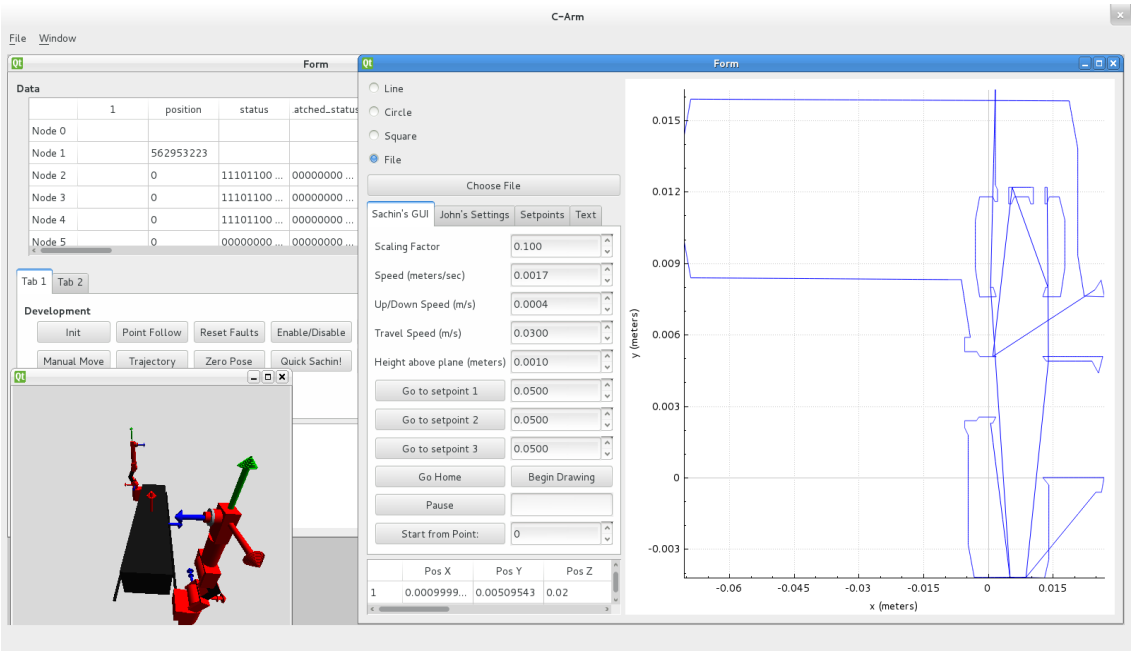

Figure 26: CORVUS extrusion and trajectory control panel GUI developed by John O'Neill (MRD Lab). Monitoring joint motion and mode of movement of the robot arm (left) and graphic showing arm movement (left bottom). Tool path visualization and setting extrusion and travel parameters (right)

Test runs were made with different values of the printing parameters in order to obtain traces of uniform bead size. The following values of the optimized printing parameters were selected for printing the test samples of a c/s of 1 mm x 1 mm:

Sl. No.	Printing Parameter	Metric
1	Corvus arm trajectory drawing speed	1.7 mm/s
2	Pen-up and pen-down speed (approach and departure from work surface in trajectory)	0.4 mm/s
3	Needle pen-up and pen-down height (from work surface)	1.0 mm
4	Corvus arm free travel (non-drawing trajectory) speed	30.0 mm
5	Corvus arm free travel height (from work surface)	20.0 mm
6	Motor start time (prior to drawing trajectory)	0.5 seconds
7	Motor stop time (in drawing trajectory)	0.1 seconds

3.2.2 Experiment 2: Characterization of conductive silicone

Experiment 1 established the feasibility of a syringe-based extrusion process for printing conductive interconnects and traces for stretchable circuits. The purpose of Experiment 2 was to (1) study the conductive behavior of the SS-26 material in the embedded silicone environment and (2) demonstrate performance characteristics of the material under a uni-axial strain.

Experimental conditions

This experiment was carried out at 7-SIGMA Inc., Minneapolis, with the collaborative permission of Wade Eichhorn, Product Manager, and with the assistance of Dave Winters, Analytical Chemist, and Jim Norris, Senior Development Technician. The operative setup consisted of TA Instruments' QA 800 Dynamic Mechanical Analysis equipment for applying a force ramp on the test samples made of the printed and embedded traces of the SS-26S in non-conductive structural silicone, and measuring strain on these samples. The Keithley Model 6514 Programmable electrometer was used for measuring the current through the conductive pathway of the trace deposited on the test sample. Recording took place while the test sample was stretched under a pre-set force ramp with the Keithley recording synced to the operation of the DMA tester.

Interfacing electrical components with conductive silicone:

A number of test samples were created both manually and with trajectory control using Corvus. 3 different methods of interfacing the conductive silicone traces with the metallic leads was used as shown in Figure 27. In method 1, header pins were used. The pins were pierced through the silicone trace and substrate and the metallic leads inserted into the pins as needed. While this method ensures there are no dangling wires on the test sample, it causes deformation in the sample due to the comparatively larger weight of the pins. Also delamination was observed during applying and removing of metallic leads. Method 2 uses direct insertion of the copper leads into the body of the conductive trace to form a continuous conductive pathway. The leads can be inserted into the trace right after or before deposition of the trace (in which case the leads need to be adequately anchored to the substrate so there is no relative motion). This can be accomplished by robotic pick-and-place or manual placement. Alternatively, the same can be done after curing of the silicone trace (the sharp lead pokes directly into the cross-section of the bead. Care must be taken during building of subsequent layers (or embedding via molding) to avoid any loose contact due to cavities at the interface). This is the method used by Periard et al. in their use of SS-26F to 3D print circuits shown in Figure 4 [10].

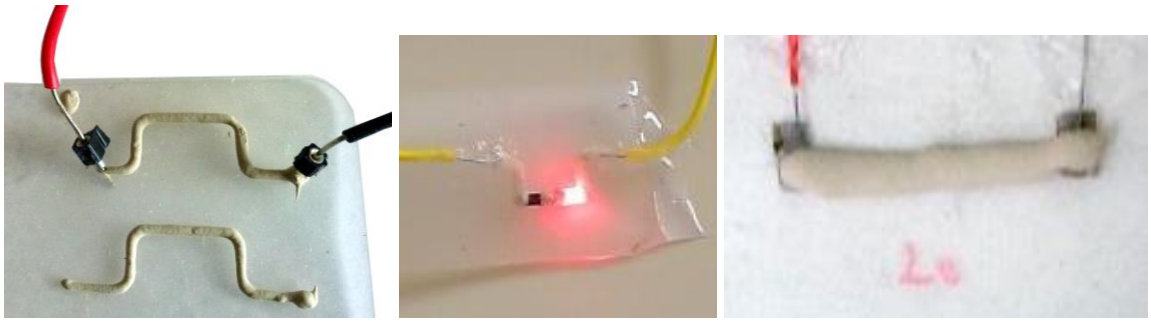

Figure 27: Methods to interface with the conductive silicone: Method 1 - Using header pins (left), Method 2 - direct insertion (center) and Method 3 - steel mesh interfaces (right)

Method 3 uses custom-prepared steel mesh contact interfaces which are soldered onto the leads and anchored on the substrate prior to printing the trace. This method ensures maximum electrical connectivity and can also isolate the strain applied on the flexible silicone, from the rigid metallic lead. It also overcomes any possible defects in the trace

deposition either due to formation of air bubbles or oil reservoirs, or due to delamination from the circular wire under stretching.

Equipment

The QA800 is a leading DMA tester utilizing non-contact linear drive technology to provide precise control of stress, with strain measurement done using an optical encoder with high resolution. It can apply a maximum force of 18N with a resolution of 0.00001N and strain resolution of 1nm. This is ideal for testing the conductive silicone material since the linear drive can be used to apply a steady force ramp on a test sample and accurately calculate the strain on the sample.

Figure 28: The TA Instruments' QA 800 DMA tester (left) and the Keithley 6514 (right) (courtesy 7-SIGMA Inc.)

The Keithley Model 6514 Electrometer combines flexible interfacing capabilities with high current sensitivity, charge measurement capabilities, resolution, and speed. It has digital I/O interfaces making it simple to configure the setup for measurement of current across a test sample in conjunction with the DMA tester.

Data collection

In order to study the behavior of the conductive silicone under increasing strain, a constant force ramp of 2N/min was applied to the test sample. Data was collected

simultaneously from the DMA test equipment and the Keithley electrometer by syncing the stretching of the test sample with the measurement of current through the sample by the Keithley. While the QA800 recorded data through a custom interface, the Keithley meter was connected to a PC and LabVIEW (by National Instruments) was used to record data. The LabVIEW setup was limited to 2000 counts of data per trial at a constant sampling rate of 10 counts/s. The QA800 also sampled at 10 Hz and recorded strain, stress and force data. The voltage across the test sample was set from the LabVIEW interface and the number of counts was set as required for the particular trial.

Analysis and Results

Preliminary testing was conducted on a 3-axis custom linear translation stage. Straight line traces with embedded electrodes were tested with a uni-axial strain to determine the validity of the clamping and mounting methods for the test samples as well to collect preliminary data on conductivity.

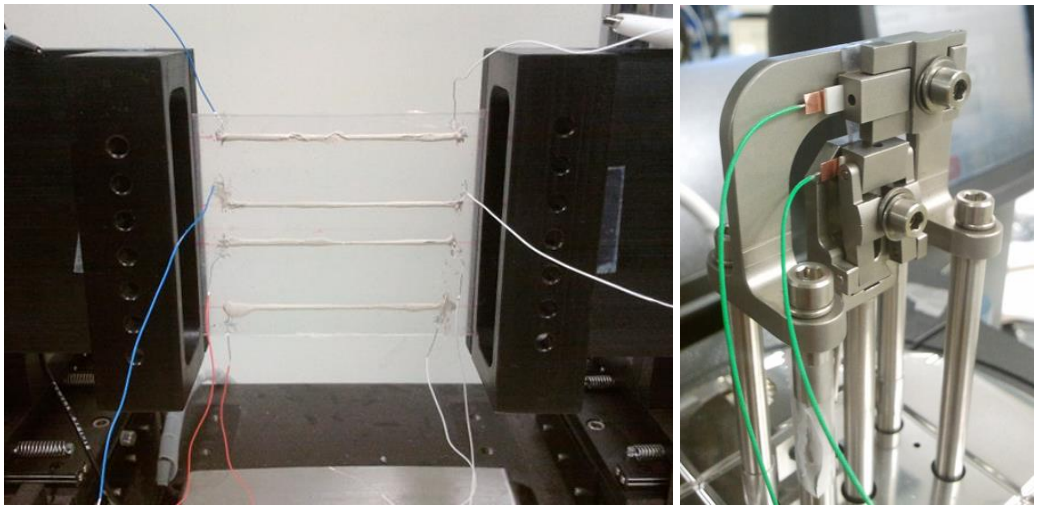

Figure 29: Initial stretch test was conducted with a custom linear slide setup with 0.01" resolution (left). An automated force ramp was later used for testing (right) using DMA Q800 tester by TA Instruments (courtesy 7-Sigma)

The figure above shows the clamping scheme for the test samples (Figure 30**)** on the QA800. Short conductive silicone traces laid on a clear silicone substrate (RTV 2-part Elastosil 40 durometer silicone, 7-Sigma), and coated with a liquid silicone rubber (2-part RTV 5 durometer silicone, 7-Sigma) upon cure, were interfaced with electrodes. In this

setup the electrode interface points of the sample were clamped under the C-clamps on the DMA tester.

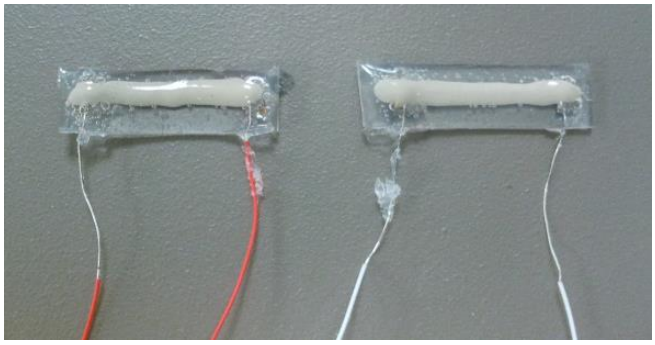

Figure 30: Test samples of conductive silicone 20 mm long with the electrode-silicone interfaces being clamped on the DMA tester. Samples were laid on a 40 durometer Silicone sheet with thin coating on top after the trace was laid for preventing delamination from the surface of the substrate

The current flow through the conductive trace under a constant applied voltage was measured in sync with the applied strain on the test sample. The resistance-strain curve is shown below with an elongation of around 25%.

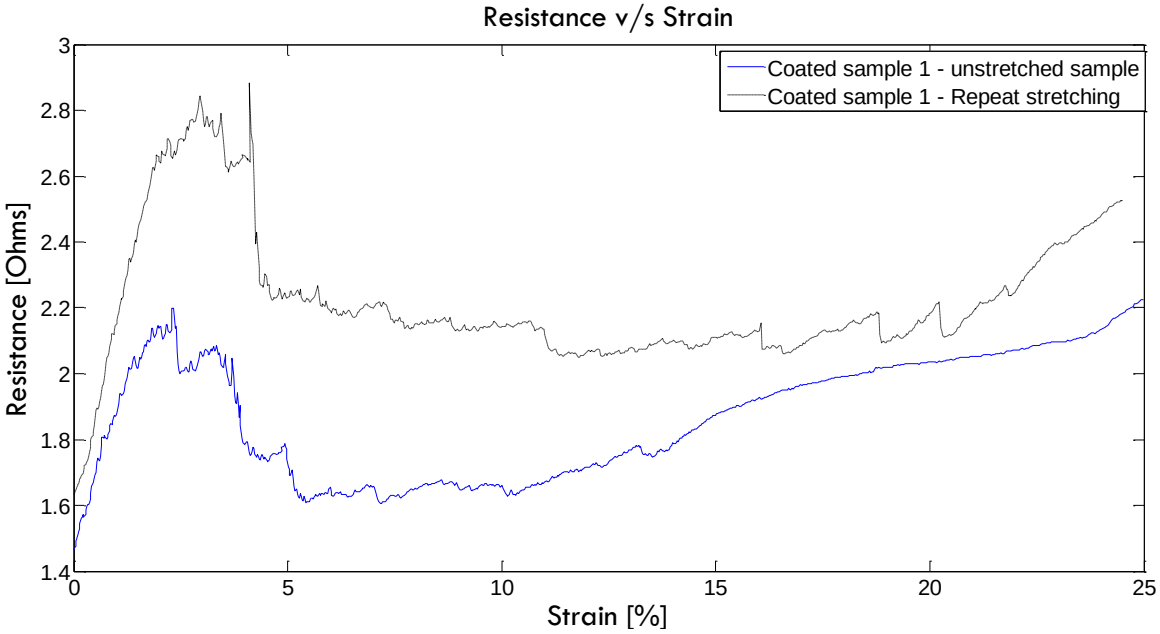

Figure 31: Resistance (y-axis) v/s strain (x-axis) behavior of the SS-26S silicone test samples

The loading of the sample was repeated, each time with a 2 N/min force ramp (blue: unstretched sample, dotted: repeat stretching). A sharp peak in the resistance was

observed under initial loading in all such samples tested. This was speculated to be due to slippage and delamination of conductive silicone at the electrode interfaces due to the difference in force applied on the sample and at the C-clamps, under which the interfaces rest. To overcome this source of experimental error the test samples were modified as shown below, with the electrodes inserted out-of-axis of the stretchable length of the SS-26S trace to avoid clamping of the electrodes at the interfaces.

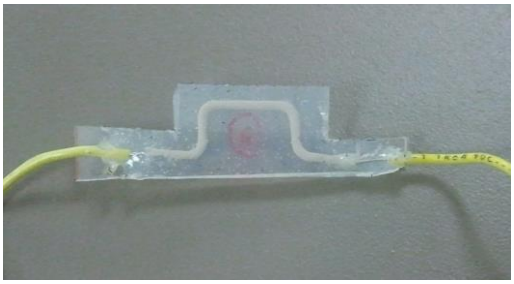

Figure 32: Modified test sample to eliminate clamping effects of the electrode-silicone interfaces with the extended U section only clamped on the DMA Q800. Trace c/s of 1mm x 1mm with a stretchable length of 12mm.

The following plot of resistance v/s strain was observed:

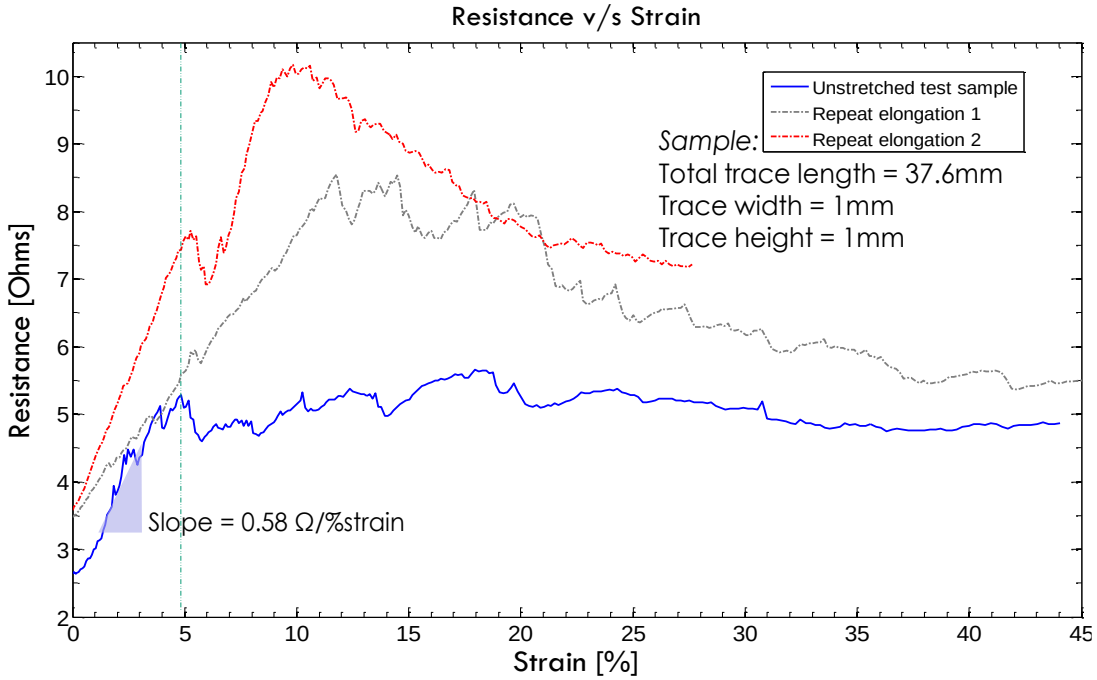

Figure 33: Variation of resistance of modified SS-26S test samples under repetition of constant force ramp loading

There is a clear indication of irreversible elongation of the sample upon relaxation, which corresponds to a marked increase in resistance at the start of each repeat test. It is interesting to note that the change in this delta resistance is lower for the second repetition (uppermost red dotted curve). There was a larger time delay in between the occurrences of the test than the first time, indicating that there is a significant time delay for the cross-linked silicone to relax nearly to its original length.

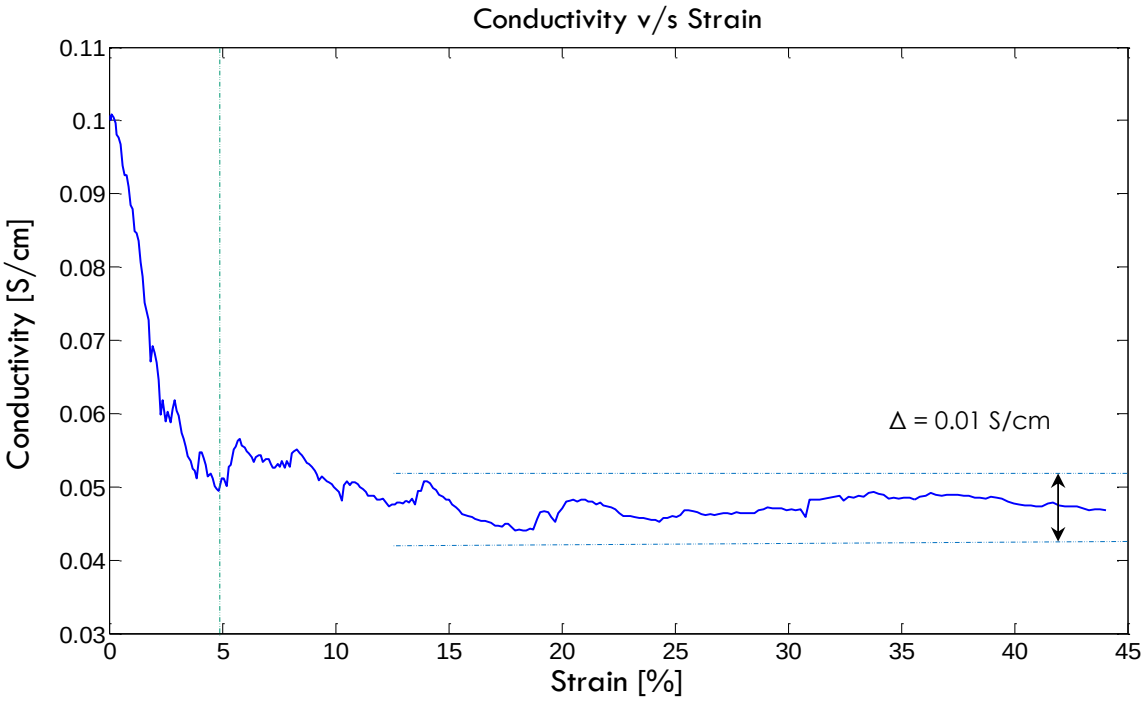

Figure 34: Plot of conductivity of the SS-26S in the modified test sample as a function of uni-axial strain

Another major observation is that the first section of the plot (Figure 33) is linear with a slope of about 0.58 ohm/ % strain (blue curve) and a peak is reached at approximately 5% strain. This behavior was observed even when repeated even though the rate of change of resistance is varied. However this is due to the time delay between occurrences of the experiment on the same sample, as curves 1 and 3 (blue and red) show similar slopes. This indicates a possible predictable linear resistance increase behavior. This implies that while the sample is initially stretched the conductivity drops at a steady rate, (which might be linked to the cross-linked polymer characteristics of the conductive and non-conductive silicone layers of the sample) beyond which it oscillates before approaching a steady state value at increased elongations (Figure 35). These samples

were stretched up to 45% elongation. However this was due to the limitation of the data recording of the Keithley, and not because of the stretchable limit of the samples, which can definitely be stretched much further.

3.2.3 Experiment 3: Printing fully-functional embedded circuits

Experiment 2 gave interesting insights into the conductive performance of the SS-26S when used as printed electrical traces. Experiment 3 takes this further by (1) by printing a complete fully functional circuit with SS-26S conductive traces and optoelectronic components in an embedded silicone environment and (2) demonstrating performance characteristics of the stretchable circuit under a uni-axial strain.
Similar to the process described in experiment 2, some sample circuits were printed to test electrical functioning of completely embedded circuits. LEDs were used as debuggers, indicating any changes in the working of these 'skins' when stretched or bent.

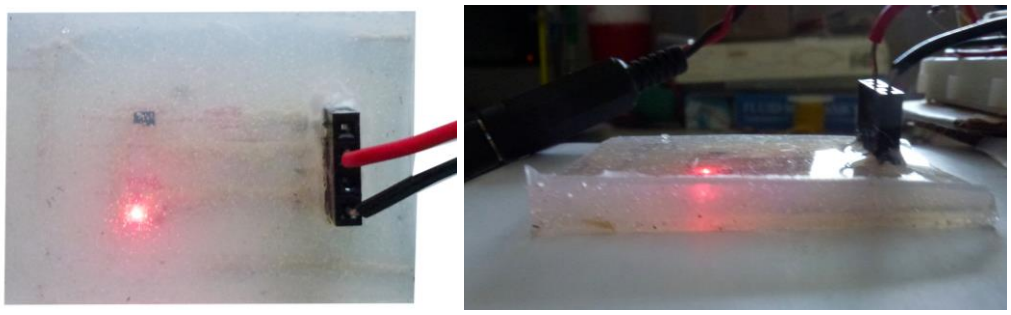

Figure 35: Testing the working of a printed, completely embedded LED circuit using an external 5V supply

Complete circuit printing

In order to test the effect of strain on a complete circuit, the voltage divider circuit was chosen as suitable candidate for 3D printing. This circuit not only contains several SMT components (1206 package) but also has an ATtiny85 8-pin microcontroller and 4-pin header for interfacing with external power supply and Bluetooth module (on a separate portable board). This also provides a wide variety of pin-silicone interfacing challenges with the variation in metallic surface form on the components as well as the pin

configurations. Tool path is planned as per required physical electrical circuit layout and converted to .svg trajectory file for CORVUS.

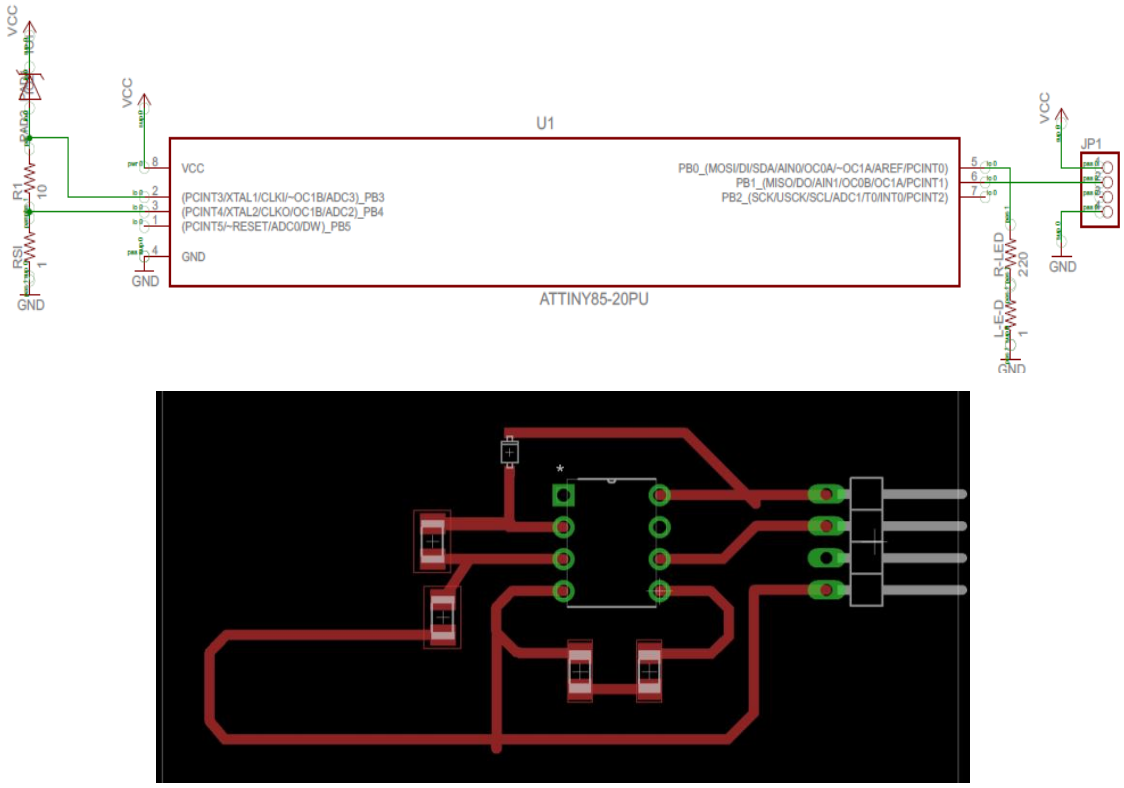

Figure 36: Schematic (top) and circuit physical layout (bottom) were developed using Eagle PCB for prototyping and testing of circuit.

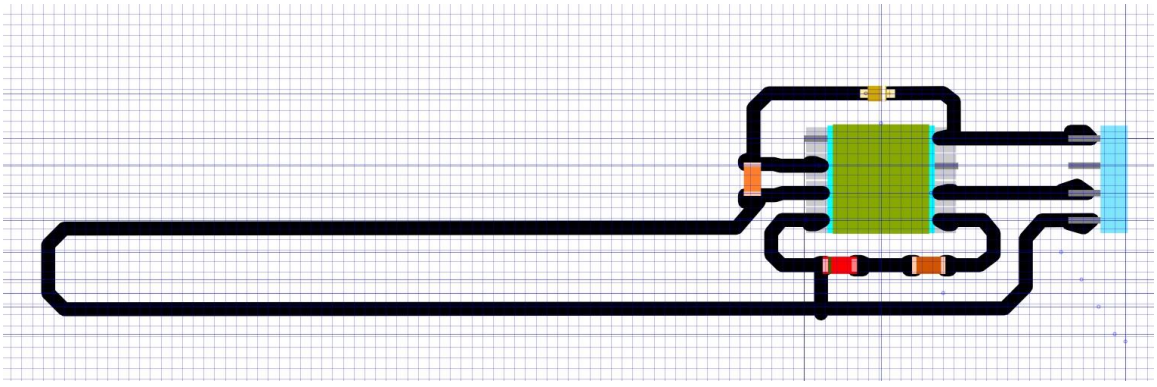

Figure 37: After the circuit physical layout was confirmed the layer-by-layer tool path was fed to CORVUS as a .svg file. Here the first layer of traces plotted in Inkscape are shown, with the long conductive trace on the left acting as a substitute for the second resistor of the voltage divider.

The ATtiny85 was previously programmed using Arduino Uno as ISP with internal 8MHz clock. The circuit utilizes the resistance of the elongated section of the printed circuit as a second resistor. A Zener diode was used to drop the voltage from the regulated +5V supply to 0.3V in order regulate current flowing through the silicone traces. This reference voltage and the output voltage from the divider were captured using ADC on pins 2 and 3. One of the pins of the AT tiny was reprogrammed as a TX pin so as to transmit serial output containing the values of the DAC outputs of the 2 voltages and the resistance calculated from the voltage divider, via a Bluetooth module (HC-06, Sparkfun Electronics) while a spare pin was used to toggle a LED every 2 seconds.

The electrical components were tested with modified pin configurations for ease of robotic 3D printing. Figure 38 shows 3 different configurations of the pins on ATtiny85.

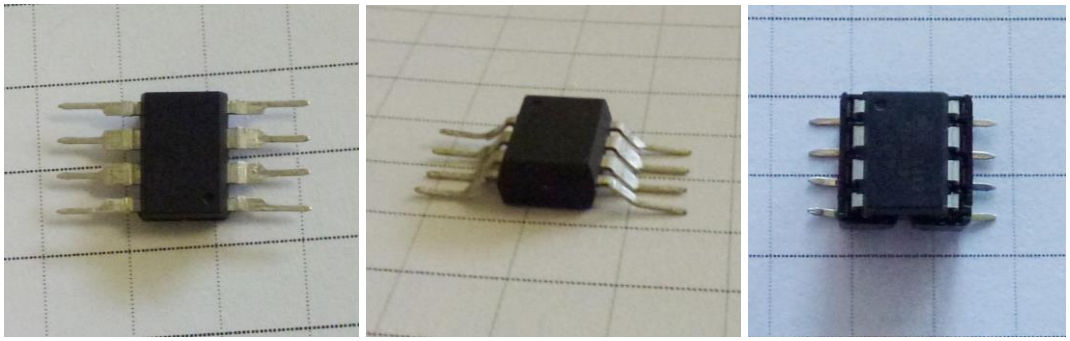

Figure 38: The ATtiny85 chip was used in various pin physical configurations to determine the ideal method for robotic printing and pick-and-place of components for a contiguous process. While the bent pins (center) allow for a shallow height with convenient strong pins for interfacing with conductive silicone traces, the use of a socket (right) allows us to remove and reprogram the chip as desired, even after the circuit is embedded in non-conductive silicone.

2 different sequences of component placement were also tested: a) silicone trace printing followed by placement of components with an additional top layer of conductive silicone added at pin interfaces to improve contact and b) place the components first followed by printing of the traces. Both methods produced functional circuits. Depending upon the application and ease of use, either could be used.

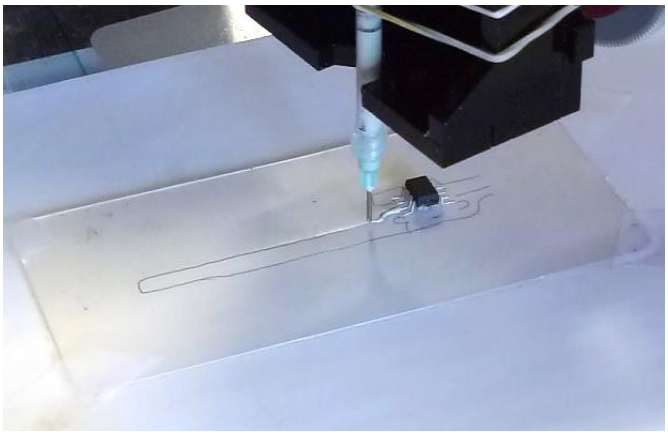

Figure 39: Printing the conductive silicone traces with a pre-placed ATtiny85 chip on flexible substrate. Tool path was modified to start extrusion at a predefined distance from the chip wall to avoid running into or moving the chip.

The completed voltage divider circuit is tested for its working under no-load, no-flex default planar condition

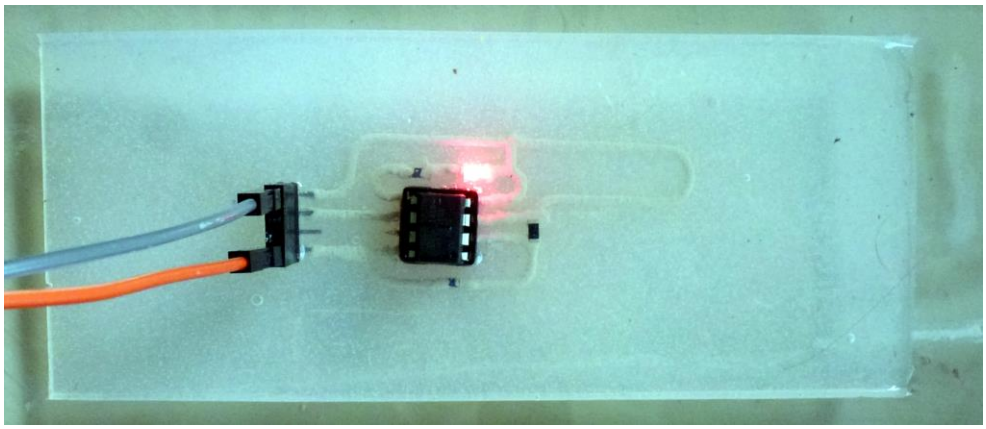

Figure 40: Demonstration of the complete voltage divider circuit (sample 1) with external regulated +5V power supply. The ATtiny85 was programmed previously using a separate portable programmer, to transmit DAC data from the voltage divider via Bluetooth. The LED toggles every 2s.

Multiple iterations of this circuit were printed for optimizing the physical layout and component interfacing of the circuit. Flat configuration of the output pin headers (in-plane with the substrate) was tested to eliminate the strain on the silicone skin from the electrodes inserted into the header in sample 1. A female-female 3-pin connector was used to then connect the skin to external power supply, Bluetooth and ground respectively as shown in Figure 44.

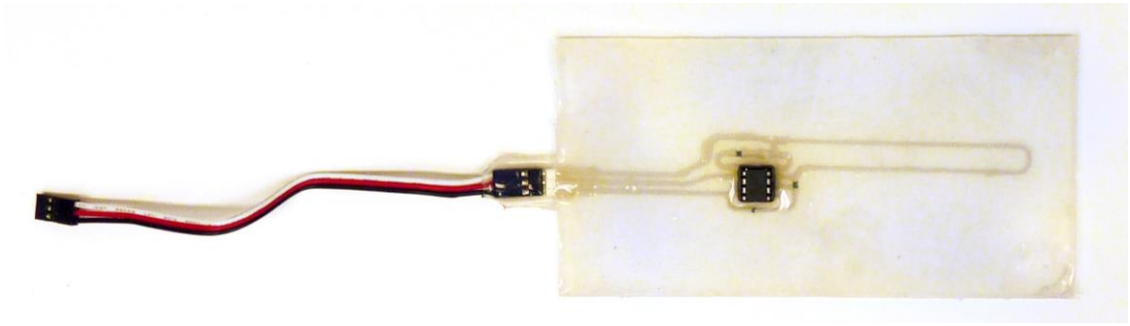

Figure 41: Voltage divider circuit 'skin' (sample 3) with flat header connector for strain relief

These sample circuits were also tested casually for their working under uncontrolled stretching or flexing as shown in figure below.

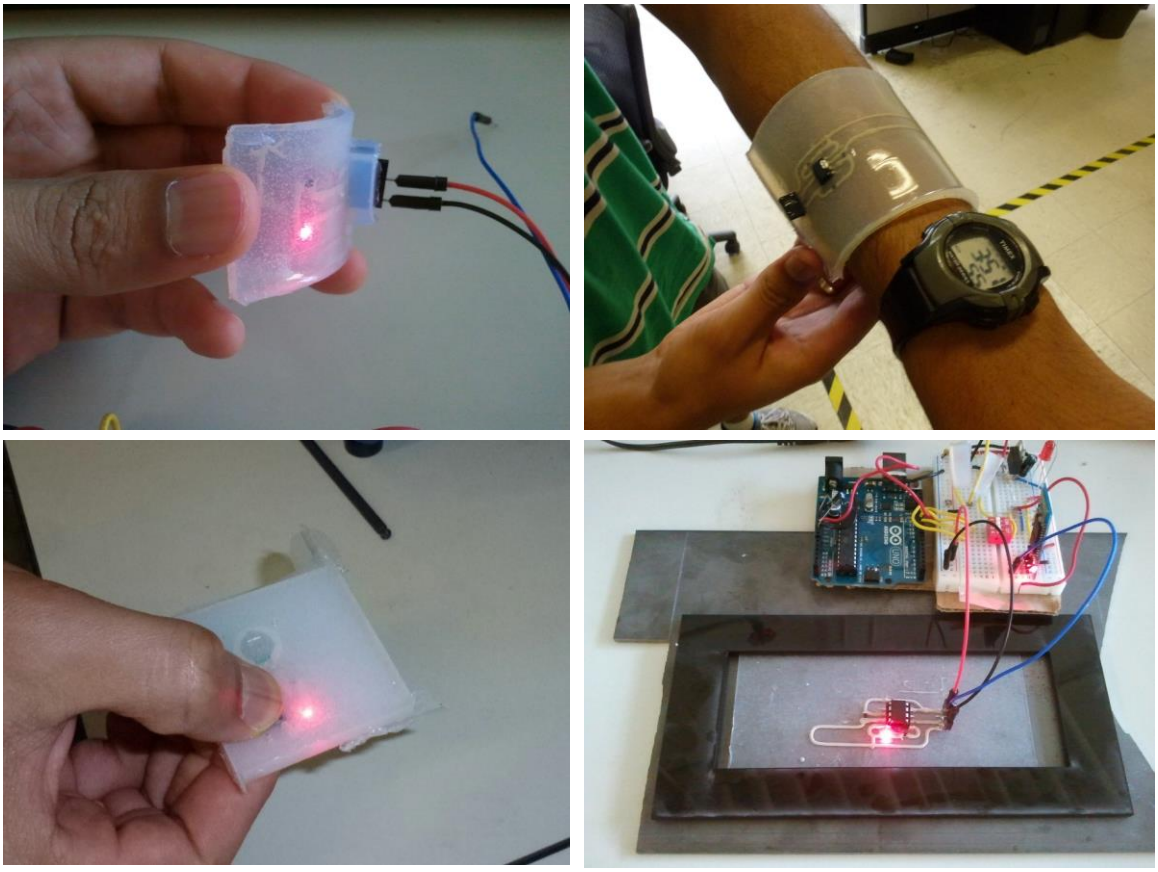

Figure 42: Demonstration of the working of LED circuit under flexion (top left). The stretchable substrate and conductive layer bend in unison and twist to conform to the mounting surface. Here the voltage divider circuit 'skin' is manipulated to conform to the user's arm (top right). (Bottom left) A completely self-contained Push-button LED circuit, with embedded LED, push-button and a 3V button battery; (bottom right) the voltage divider circuit in use

Experimental setup

A custom test rig (Figure 43) was setup to test the behavior of the voltage divider embedded circuit under stretching. Two co-axial linear slide stages were mounted on a rigid platform to avoid vibrations and maintain strain along a single axis.

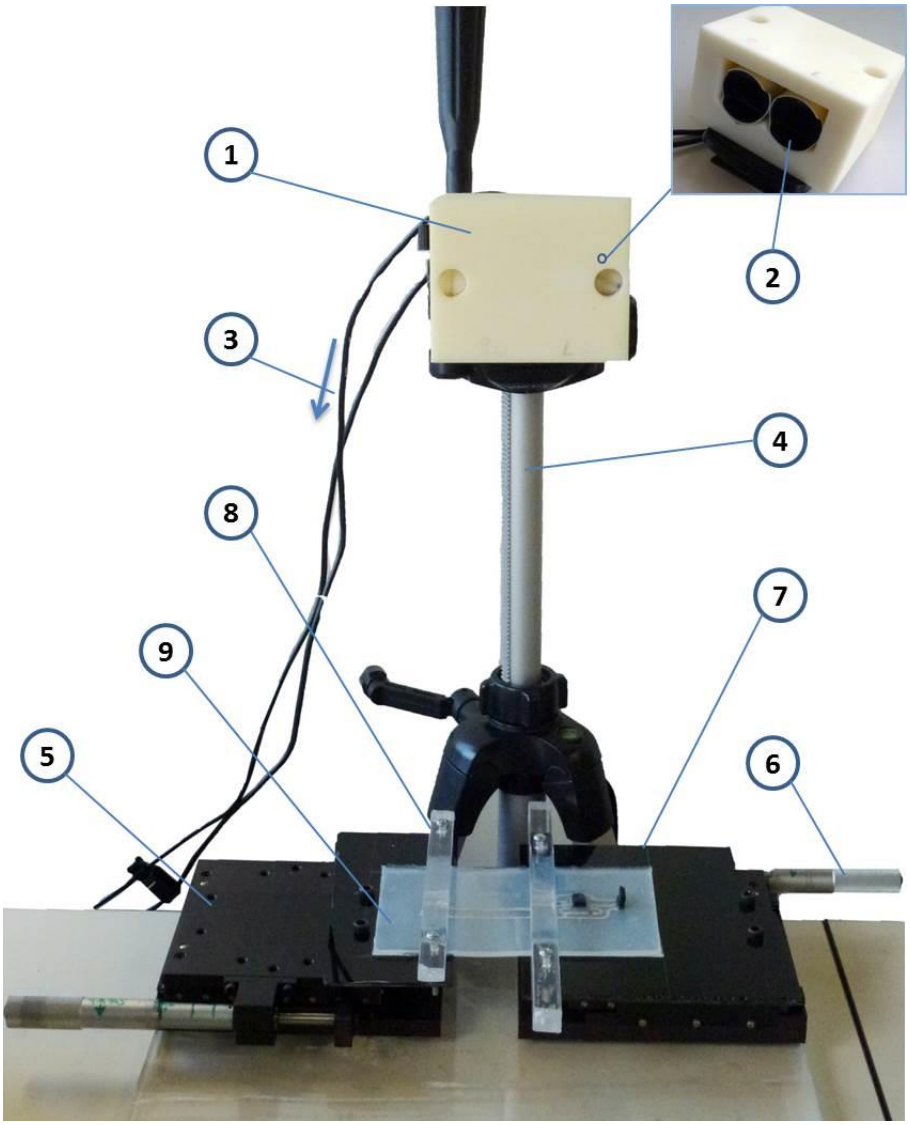

Figure 43: Custom testing rig developed to test behavior of printed circuits under strain: 1) Camera housing for 2 USB cameras (inset), 2) HD camera for tracking motion of sample, 3) Cable out to computer USB 3.0, 4) Tripod for mounting the camera housing – can be altered to adjust the field of vision of the camera, 5) linear translation stage with a mounting platform, 6) Rotary control for linear slide, 7) mounting plate on linear slide platform, 8) slender clamps to constrain and grip the test sample (9).

The linear slides have a resolution of 0.01 inches. The embedded circuit ‘skin’ was mounted on the linear stage and clamped to prevent slipping. The clamps were provided with minor cutouts to prevent application of force on the skin at the site of the conductive traces to avoid any possible squishing actions. The right stage was kept fixed while the left stage was movable. A constant smooth feed was maintained via one of the linear slides to cause elongation of the sample embedded circuit. The separation of the clamps was monitored via a camera (Microsoft Life Studio 1080p HD USB camera) mounted in a separate housing on a tripod. Blue and red markers were used to track the stretching using a computer vision algorithm.

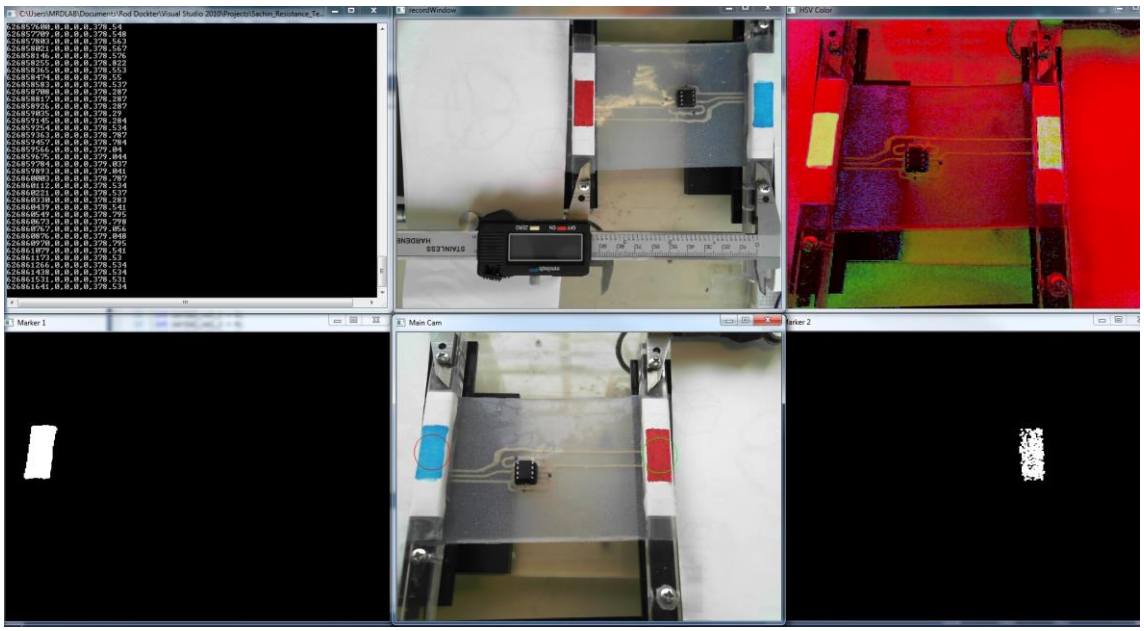

Figure 44: Screenshot of distance tracking of the test embedded circuit: (clockwise from the top left) HSV gradation as determined from the camera; actual image captured with 2 markers to track the translation; selected hue identification (red) of the right clamp and left clamp (blue) respectively. (Software courtesy of Rod Dockter)

Analysis and Results

To extract the location of the colored markers on each frame from the video stream of the HD USB camera, hue identification using HSV color scale was implemented. Using a setup window the two colors of the markers were fed to the program by adjusting HSV sliders so as to selectively identify each hue separately and calculate the average center

location of the mark on the clamp. The pixel separation between the two locations was then calculated and integrated with the serial output of the voltage divider circuit, along with the timestamp data into a single text file. This data was then unpacked to plot the resistance calculated from the voltage divider with the percent elongation.

Initially a limit test was done to determine the working limit of a circuit with 1206 package electrical components (330 ohm resistor and a red LED) connected with traces of the conductive silicone. The sample was stretched slowly checking to see if the LED still worked. It was observed that **the circuit functioned up to at an elongation of 60%**. The circuit stopped working at 60% strain because of separation of the conductive silicone trace from the component due to delamination. However on bringing the sample back to its original length, re-lamination took place allowing the LED to glow again.

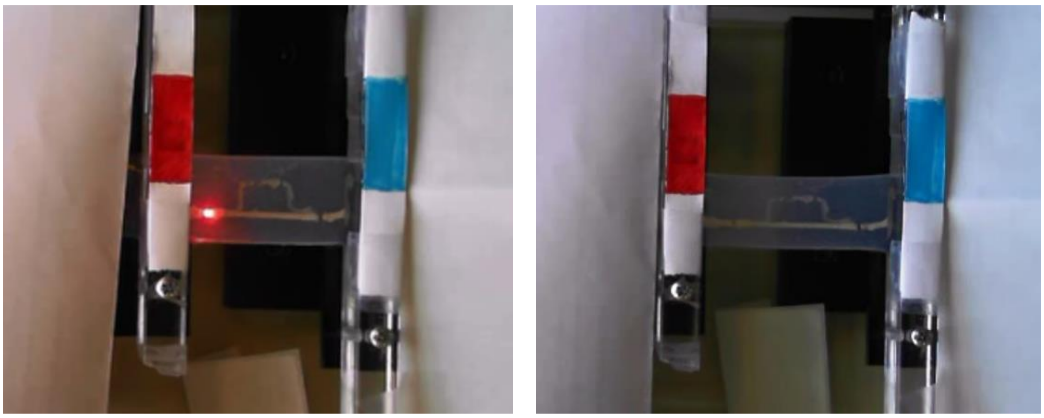

Figure 45: The LED circuit (connected to external power supply) at original length (left) is stretched till it stops working at 60% strain (right)

Using the same setup the voltage divider ‘skin’ test sample was clamped at either end of the silicone sheet with the embedded electronics in the middle (Figure 44). The sample was subjected to one cycle of stretching and relaxation with a time gap of one minute in between to observe any transient behavior of the resistance of the conductive silicone. Figure 47 shows plots of the output and reference voltages from the voltage divider, measured via ADC from the ATtiny85. The green curve shows the strain ramp function. The plot on the right shows resistance as a function of time.

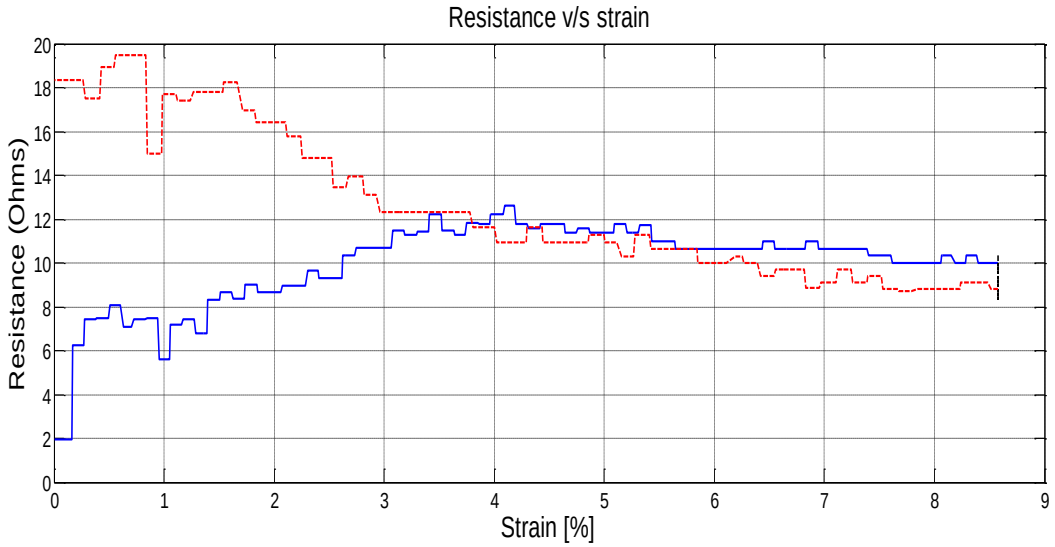

Figure 46: Resistance calculated by the voltage divider circuit plotted against the strain. Curves: Initial stretching (blue), constant elongation at 8.7% (10mm) (black) and subsequent relaxation to original length (red).

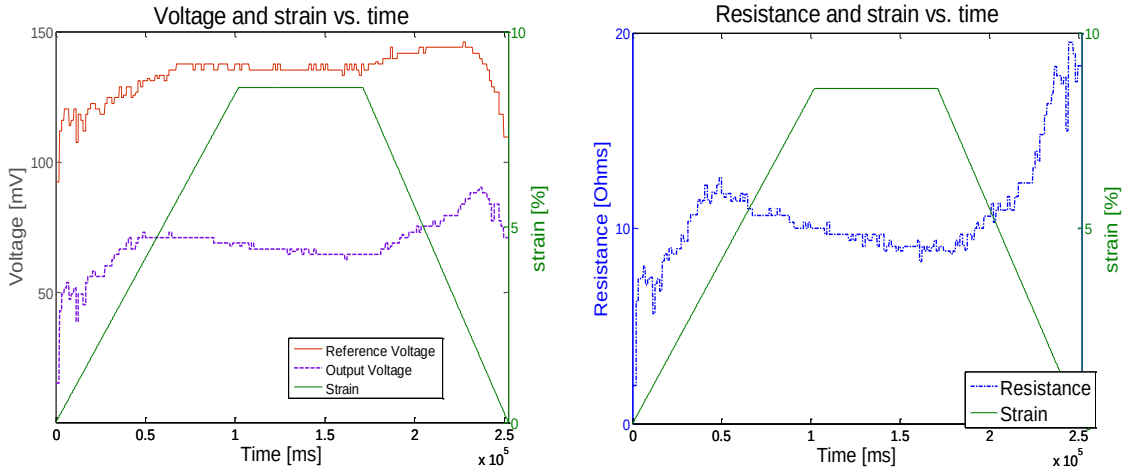

Figure 47: Plots of the reference and output voltages (left) and resistance v/s time for 1 cycle of stretching, constant elongation and relaxation

Figure 46 shows resistance vs. strain. As the sample is stretched, the resistance increases nearly linearly before peaking and upon further stretching the resistance starts to drop before leveling out. When the 8.7% elongation is maintained for a minute, the resistance is found to decay and drop from 10 ohms to 8.5 ohms. As the relaxation starts the resistance starts to rise before rising drastically as the sample approaches its original length.

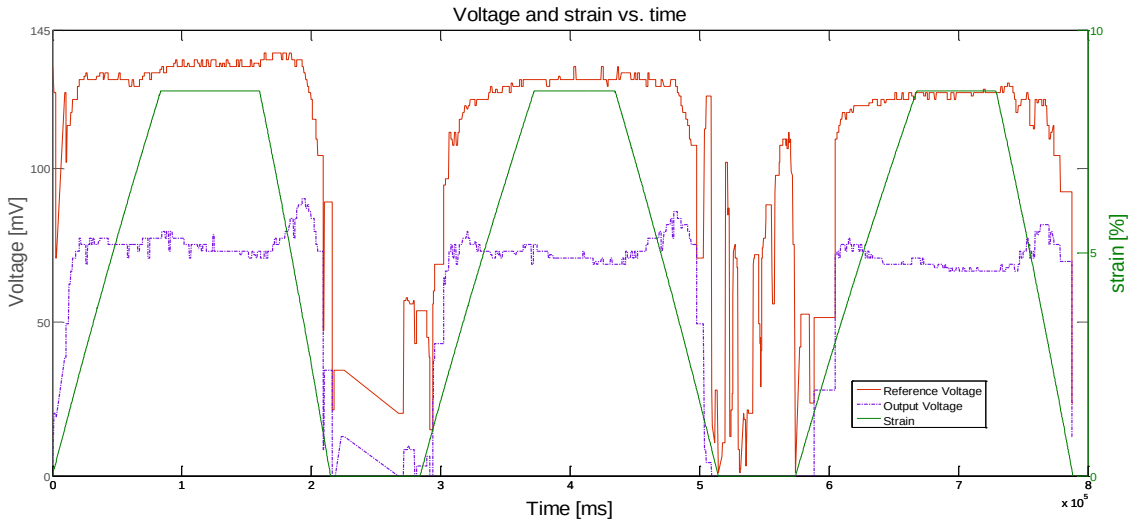

Figure 48: Tracking the changes in the reference and output voltages as a function of time for 3 cycles of strain applied as a ramp function.

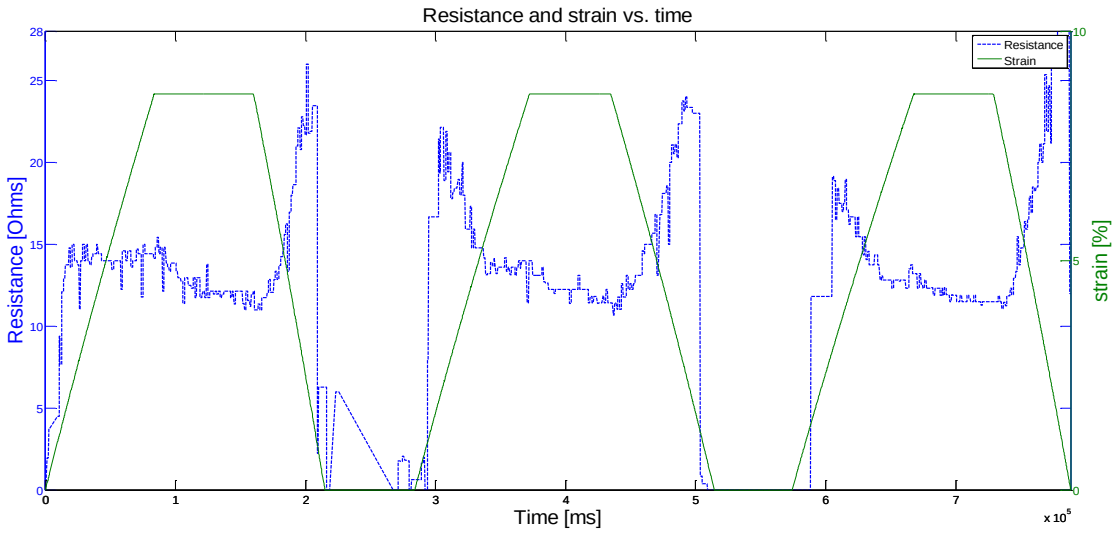

Figure 49: Variation of resistance with time over 3 cycles of stretching and relaxing from to and from an elongation of 8.7%. (Strain shown in green)

When the experiment was conducted over a number of cycles of stretching and relaxation with time delays in between to observe transients, similar behavior was observed over each cycle. As is evident from the voltage curve (Figure 48) the reference voltage appears to drastically change or drop to zero as the sample is brought back to its original length from a high strain. This is possibly due to the delamination and loss of electrical contact of the conductive traces to the leads of the Zener diode used to drop the regulated power

supply from 5V to 0.3V. Due to the small package specifications of the diode used (electrode size: 0.4mm x 0.25 mm, height 0.25mm) there is considerable strain on the interface with the conductive silicone causing separation under relaxation. It is proposed that use of a flexible but stiff mesh or harder rubber islands for housing surface mount components with packages smaller than 1206 would help isolate the strain from the rigid components and alleviate the problem caused due to loss of electrical signal at the interface.

Chapter 4

Conclusion

In this work we have successfully tested the feasibility of a syringe extrusion-based 3D printing process to print stretchable embedded electronics through the use of SS-26S conductive silicone on flexible non-conductive silicone substrates. Instead of merely using the conductive silicone traces as flexible interconnects, this method used the conductive material for creating complete circuitry with SMT components and embedded microcontrollers.

The electrical conductivity of the SS-26S silicone with silver filler was studied through material characterization tests and found to be satisfactory for creation of integrated circuits. The variation of the resistance with strain was mapped to understand the effect of elongation on electrical performance. Completely functional integrated circuits with added optoelectronic components were successfully printed using the 6-axis robot CORVUS with a custom-designed syringe extrusion head and found to function well electronically under applied stretching and flexion. This validates the capability of 3D printing to manufacture fully functional embedded circuits capable of functioning under considerable strain and bending.

From research and testing of various methods for interfacing between electrical components and the conductive silicone, it is determined that the reliability of the performance could be improved further by ensuring adequate and constant contact for formation of suitable electrically conductive pathways in the circuit. This can be achieved through isolation of electrical components from applied strain, either through the use of multiple durometer structural silicones or via non-conductive surface meshes for housing the components and providing strain relief.

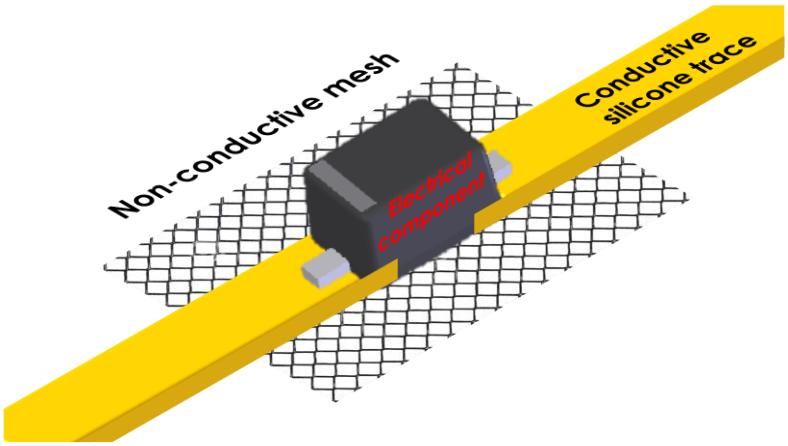

Figure 50: Use of non-conductive mesh for strain relief and to improve contact between component electrode and conductive silicone trace

There is considerable scope for future work in optimizing this manufacturing process and fine-tuning the material selection and curing, including design of a dedicated dual-cure system capable of simultaneously curing the conductive RTV silicone and structural UV cured non-conductive silicone, for enhanced manufacturability and improved high-speed printing ability. Further tests can be performed for build and testing of a complete ‘skin-like’ device like a surgical instrumented glove with printed embedded sensors and miscellaneous electrical components, custom-built to fit the anatomical geometry of a clinician’s hand, utilizing the capability of CORVUS to track human anatomy and print on complex and irregular surfaces.

Bibliography

[1] Tentzeris MM, Nikolaou S. RFID-enabled ultrasensitive wireless sensors utilizing inkjet-printed antennas and carbon nanotubes for gas detection applications. In: Microwaves, Communications, Antennas and Electronics Systems, 2009. COMCAS 2009. IEEE International Conference on. IEEE; 2009. p. 1–5.

[2] Ahn BY, Duoss EB, Motala MJ, Guo X, Park SI, Xiong Y, et al. Omnidirectional printing of flexible, stretchable, and spanning silver microelectrodes. Science. 2009;323(5921):1590–1593.

[3] Fan Z, Ho JC, Takahashi T, Yerushalmi R, Takei K, Ford AC, et al. Toward the development of printable nanowire electronics and sensors. Advanced Materials. 2009;21(37):3730–3743.

[4] Rogers JA, Someya T, Huang Y. Materials and mechanics for stretchable electronics. Science. 2010;327(5973):1603–1607.

[5] Vervust T, Buyle G, Bossuyt F, Vanfleteren J. Integration of stretchable and washable electronic modules for smart textile applications. Journal of The Textile Institute. 2012;103(10):1127–1138.

[6] Cao Q, Kim Hs, Pimparkar N, Kulkarni JP, Wang C, Shim M, et al. Medium-scale carbon nanotube thin-film integrated circuits on flexible plastic substrates. Nature. 2008;454(7203):495–500.

[7] Axisa F, Brosteaux D, De Leersnyder E, Bossuyt F, Vanfleteren J, Hermans B, et al. Biomedical stretchable sytems using mid based stretchable electronics technology. In: Engineering in Medicine and Biology Society, 2007. EMBS 2007. 29th Annual International Conference of the IEEE. IEEE; 2007. p. 5687–5690.

[8] Abu-Khalaf JM, Park JW, Mascaro DJ, Mascaro SA. Stretchable fingernail sensors for measurement of fingertip force. In: EuroHaptics conference, 2009 and Symposium on Haptic Interfaces for Virtual Environment and Teleoperator Systems. World Haptics 2009. Third Joint. IEEE; 2009. p. 625–626.

[9] Kramer RK, Majidi C, Wood RJ. Wearable tactile keypad with stretchable artificial skin. In: Robotics and Automation (ICRA), 2011 IEEE International Conference on. IEEE; 2011. p. 1103–1107.

[10] Periard D, Malone E, Lipson H. Printing embedded circuits. In: Proceedings of the 18th Solid Freeform Fabrication Symposium, Austin TX. Society of Manufacturing Engineers; 2007. p. 503–12.

[11] Mannoor MS, Jiang Z, James T, Kong YL, Malatesta KA, Soboyejo WO, et al. 3D printed bionic ears. Nano letters. 2013;13(6):2634–2639.

[12] O'Neill JJ, Kowalewski TM. Online Free Anatomy Registration via Non-Contact Skeletal Tracking for Collaborative Human/Robot Interaction in Surgical Robotics. Journal of Medical Devices. 2014;.

[13] Wagner S, Bauer S. Materials for stretchable electronics. Mrs Bulletin. 2012;37(03):207–213.

[14] Keplinger C, Sun JY, Foo CC, Rothemund P, Whitesides GM, Suo Z. Stretchable, Transparent, Ionic Conductors. Science. 2013;341(6149):984–987.

[15] Kim Y, Zhu J, Yeom B, Di Prima M, Su X, Kim JG, et al. Stretchable nanoparticle conductors with self-organized conductive pathways. Nature. 2013;500(7460):59–63.

[16] Kim DH, Xiao J, Song J, Huang Y, Rogers JA. Stretchable, curvilinear electronics based on inorganic materials. Advanced Materials. 2010;22(19):2108–2124.

[17] MDDI. Using Polyurethanes in Medical Applications; 2006. Available from: http://www.mddionline.com/article/using-polyurethanes-medical-applications.

[18] Ostmann A, Loher T, Seckel M, Bottcher L, Reichl H. Manufacturing concepts for stretchable electronic systems. In: Microsystems, Packaging, Assembly & Circuits Technology Conference, 2008. IMPACT 2008. 3rd International. IEEE; 2008. p. 24–27.

[19] Axisa F, Brosteaux D, De Leersnyder E, Bossuyt F, Gonzalez M, De Smet N, et al. Low cost, biocompatible elastic and conformable electronic technologies using MID in stretchable polymer. In: Engineering in Medicine and Biology Society, 2007. EMBS 2007. 29th Annual International Conference of the IEEE. IEEE; 2007. p. 6592–6595.

[20] ; Method for manufacturing a stretchable electronic device. ; 2012. US Patent 8,207,473.

[21] Bossuyt F, Vervust T, Axisa F, Vanfleteren J. A new low cost, elastic and conformable electronics technology for soft and stretchable electronic devices by use of a stretchable substrate. In: Microelectronics and Packaging Conference, 2009. EMPC 2009. European. IEEE; 2009. p. 1–6.

[22] Brosteaux D, Axisa F, Gonzalez M, Vanfleteren J. Design and fabrication of elastic interconnections for stretchable electronic circuits. Electron Device Letters, IEEE. 2007;28(7):552–554.

[23] Sekitani T, Noguchi Y, Hata K, Fukushima T, Aida T, Someya T. A rubberlike stretchable active matrix using elastic conductors. Science. 2008;321(5895):1468–1472.

[24] Park M, Im J, Shin M, Min Y, Park J, Cho H, et al. Highly stretchable electric circuits from a composite material of silver nanoparticles and elastomeric fibres. Nature nanotechnology. 2012;7(12):803–809.

[25] Thompson B, Yoon HS. Aerosol printed carbon nanotube strain sensor. In: Proceedings of SPIE. vol. 8346; 2012. p. 83461C.

[26] Dimitrov D, Schreve K, De Beer N. Advances in three dimensional printing–state of the art and future perspectives. Rapid Prototyping Journal. 2006;12(3):136–147.

[27] Giannatsis J, Dedoussis V. Additive fabrication technologies applied to medicine and health care: a review. The International Journal of Advanced Manufacturing Technology. 2009;40(1-2):116–127.

[28] Gibson I, Cheung L, Chow S, Cheung W, Beh S, Savalani M, et al. The use of rapid prototyping to assist medical applications. Rapid Prototyping Journal. 2006;12(1):53–58.

[29] Winder J, Bibb R. Medical rapid prototyping technologies: state of the art and current limitations for application in oral and maxillofacial surgery. Journal of Oral and Maxillofacial Surgery. 2005;63(7):1006–1015.

[30] Petzold R, Zeilhofer HF, Kalender W. Rapid prototyping technology in medicine—basics and applications. Computerized Medical Imaging and Graphics. 1999;23(5):277–284.

[31] Rengier F, Mehndiratta A, von Tengg-Kobligk H, Zechmann CM, Unterhinninghofen R, Kauczor HU, et al. 3D printing based on imaging data: review of medical applications. International journal of computer assisted radiology and surgery. 2010;5(4):335–341.

[32] Pfister A, Landers R, Laib A, Hübner U, Schmelzeisen R, Mülhaupt R. Biofunctional rapid prototyping for tissue-engineering applications: 3D bioplotting versus 3D printing. Journal of Polymer Science Part A: Polymer Chemistry. 2004;42(3):624–638.

[33] Mironov V, Boland T, Trusk T, Forgacs G, Markwald RR. Organ printing: computer-aided jet-based 3D tissue engineering. TRENDS in Biotechnology. 2003;21(4):157–161.

[34] MDDI. UV-Curing Silicone Rubbers Enable New Medical Concepts and Part Designs; 2013. Available from: http://www.mddionline.com/article/uv-curing-silicone-rubbers-enable-new-medical-concepts-and-part-designs.

[35] von Muenchhausen H, Schittko F. Investigation of the outgassing process of silicone rubber. Vacuum. 1963;13(12):549–553.

[36] Li M, Tang L, Xue F, Landers R. Numerical Simulation of Ram Extrusion Process for Ceramic Materials. In: Proceedings of Solid Freeform Symposium, Austin, TX; 2011. p. 290–308.

[37] Deuser BK, Tang L, Landers RG, Leu MC, Hilmas GE. Hybrid Extrusion Force-Velocity Control Using Freeze-Form Extrusion Fabrication for Functionally Graded Material Parts. Journal of Manufacturing Science and Engineering. 2013;135(4):041015.